American Mineralogist, Volume 84, pages 821–837, 1999

Geochemistry, petrology, and cooling history of 14161,7373: A plutonic lunar sample with textural evidence of granitic-fraction separation by silicate-liquid immiscibility

B.L. JOLLIFF,[1,*] C. FLOSS,[1] I.S. MCCALLUM,[2] AND J.M. SCHWARTZ[2]

[1]Department of Earth and Planetary Sciences and the McDonnell Center for the Space Sciences, Washington University, St. Louis, Missouri 63130, U.S.A.

[2]Department of Geological Sciences, Box 351310, University of Washington, Seattle, Washington 98195, U.S.A.

ABSTRACT

We report new findings related to sample 14161,7373, the first analyzed lunar intrusive rock to show textural evidence for the formation of granitic material by silicate liquid immiscibility (SLI) and geochemical evidence for separation of that material, at least on a small scale, from mafic residua. Ion microprobe analyses of rare-earth element (REE) concentrations in silicates record the compositional evolution of this late-stage assemblage. For a sample whose bulk assemblage, that of whitlockite monzogabbro, has REE concentrations at ~5–6× KREEP levels, the silicates have only moderately high REE concentrations. The calculated REE concentrations of melt in equilibrium with pigeonite, after re-integration of pigeonite host and augite lamellae, is approximately 2× high-K KREEP. The high bulk REE concentrations of the assemblage are the result of a high proportion of whitlockite, probably an excess, i.e., the assemblage is a whitlockite cumulate. Variations in silicate REE concentrations reflect the co-crystallization of whitlockite, which we interpret to have begun crystallizing prior to the onset of late-stage immiscibility of the felsic melt fraction. Calculated cooling rates, based on a quantitative model of pyroxene exsolution, reveal a two-stage thermal history, which involved initial crystallization at a minimum depth of 700–800 m during which the primary augite and pigeonite grains unmixed to form the observed host-lamella pairs. Unusual compositional profiles close to the host-lamella interface are consistent with a second stage of mild reheating followed by rapid cooling at a depth of ~30 m, most likely in an ejecta blanket. The shallow depth of origin indicated for 14161,7373 is consistent with other studies of evolved lunar intrusive rocks, supporting the interpretation that lunar QMD and granite, as found among the Apollo samples, are late-stage differentiates of high-level intrusions and are not related to differentiation of deep crustal KREEP reservoirs.

INTRODUCTION

Although evolved lithologies are rare among lunar samples, they have assumed a disproportionate importance because they are the products of extensive differentiation processes that occurred early in lunar history and, as such, they provide critical evidence on the magmatic processes that shaped the early Moon. Among the more interesting evolved lithologies are the rocks known as quartz monzodiorite/monzogabbro (QMD/QMG) and granite/felsite, which commonly occur together (Ryder 1976; Quick et al. 1977; Warren et al. 1983; Marvin et al. 1990; Morris et al. 1990). Silicate liquid immiscibility (SLI) has been proposed as a process that might have produced lunar granite and QMD as conjugate immiscible pairs (e.g., Rutherford et al. 1976; Taylor et al. 1980; Warren et al. 1983) that separated to form the felsic and mafic components of lunar residual melts [e.g., "BaK" and "REEP" (Quick and Albee 1976), and "K-frac" and "REEP-frac," respectively (Neal and Taylor 1989c, 1991)]. Furthermore, one or the other of these components has been inferred to be the agent of metasomatism of, for example, magnesian-suite rocks (Neal and Taylor 1989a, 1989c, 1991) or autometasomatism (Jolliff et al. 1993), or to have been an important assimilant at depth in the lunar crust (Shervais et al. 1985; Longhi 1981; Warren 1988).

Important questions related to SLI in lunar plutonic settings that remain unanswered are (1) at what depths did the process of immiscible-liquid separation occur, (2) how concentrated in incompatible elements were lunar residual melts at the time of immiscible-liquid separation, (3) what was the spatial extent and scale of separation, and (4) how effective were such separated melt fractions as metasomatizing agents in the lunar crust? An over-arching question is whether or not KREEP reservoirs experienced late-stage liquid immiscibility and large-scale separation of mafic and felsic materials (see Warren et al. 1983; Neal and Taylor 1989a, 1989c; Longhi 1990; Jolliff 1998). In the laboratory, immiscibility has been produced experimentally in Fe-rich, KREEP-like compositions at pressures up to 3 kilobars (e.g., Rutherford et al. 1976, 1996; Hess et al. 1989; Longhi 1990). Textures reflecting SLI have been observed in the late-stage, iron-rich mesostasis of mare basalts (Roedder and Weiblen 1971), and numerous examples have been found of coexisting felsic and mafic glasses or breccia components, suggesting petrogenetic relationships between the felsic and mafic components (e.g., Quick et al. 1977; Morris et al. 1990). However, to date, only one lunar sample, 14161,7373, a whitlockite-rich monzogabbro, shows compel-

*E-mail: blj@levee.wustl.edu

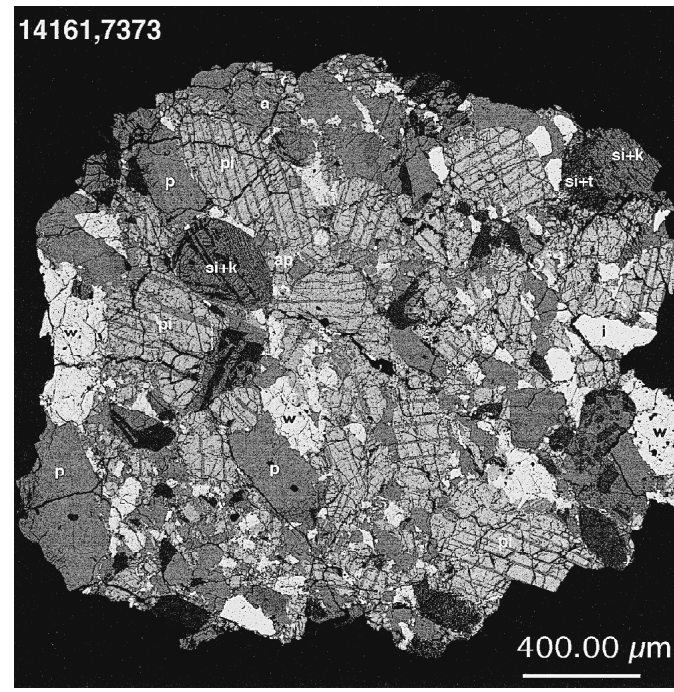

FIGURE 1. Backscattered electron (BSE) image of 14161,7373 whitlockite monzogabbro. The darkest phase is silica (si), plagioclase (p) and potassium feldspar (k) are dark gray, pigeonite (pi) and augite (a) are medium gray with augite slightly darker than pigeonite; whitlockite (w) and apatite (ap) are light gray, ilmenite (i) and zircon (z) are bright. Troilite (t) is very bright, forming tiny grains in silica-rich masses and thin stringers filling fractures. The grain marked si+t is one of several grains composed of silica and a fine "emulsion" of troilite blebs. The "egg"-shaped ovoid granophyre is marked si+k (upper left), and another one shaped like an eggplant (not marked) is present at lower right adjacent a large whitlockite grain (w). Others are present, but less prominent.

ling petrographic evidence for liquid immiscibility in a single, monomict, plutonic (intrusive) assemblage (Jolliff 1991). In an ion-microprobe study of the phosphates from this sample, Jolliff et al. (1993) presented a geochemical model for its late-stage crystallization history. In this paper, we present the results of ion-microprobe analyses of pyroxene and feldspar in 14161,7373 that further constrain the timing of crystallization of minerals in this assemblage and the variation of REE concentrations in residual melt as the assemblage crystallized. We present detailed compositional profiles of the exsolved pyroxene grains, which are used to constrain the depth of crystallization of the sample and the subsequent thermal history that this sample experienced. To date, most information on the depths of crystallization of lunar igneous samples was obtained indirectly from models of the distribution of ejecta associated with multi-ring basins (Spudis 1993). A more precise knowledge of the depths at which lunar crustal rocks crystallized or recrystallized is important not only in the reconstruction of primitive lunar stratigraphy, but also in constraining petrologic models of lunar magmatic evolution. Because conventional geobarometers are of little value on the Moon because of the low pressures, we apply the method outlined by McCallum and O'Brien (1996) in which cooling rates are determined from the width, spacing, orientation, and composition of exsolution lamellae in pyroxene.

SAMPLE DESCRIPTION

Sample 14161,7373 is a small fragment, originally 18.4 mg, of a whitlockite-rich "monzogabbro" assemblage described initially by Jolliff (1991). It was discovered during the compositional survey phase of a study of lithic fragments in Apollo 14 soils (Jolliff et al. 1991). Although shocked and fractured, it retains an igneous texture, is medium-grained and holocrystalline, has exsolved pyroxene (Fig. 1), and is demonstrably monomict (pristinity confidence class 7, Warren 1993). Grain sizes of some pigeonite, plagioclase, and whitlockite grains exceed 500 μm, potassium feldspar and silica grains range up to 200 μm, and granophyric intergrowths of potassium feldspar and silica, to 400 μm (Fig. 1). Individual mineral grains are generally anhedral. As we discuss in a later section, original cumulus textures may have been modified during solidification or impact.

The assemblage contains ~47 vol% pyroxene, 26% plagioclase, and some 27% minor and accessory minerals, including whitlockite, apatite, potassium feldspar, silica, ilmenite, zircon, and troilite (Fig. 1). The large pyroxene grains form a nearly interconnected network with other minerals mostly filling the interstices, imparting the appearance of a microcumulate. Individual pyroxene grains in this assemblage are not in optical continuity as can be seen by the orientation of exsolution lamellae in Figure 1. The assemblage also has an unusually high proportion of whitlockite (~8%) and, as a result, contains the highest measured concentrations of REE of any polymineralic lunar assemblage reported to date (Jolliff 1991).

The sample also contains compelling textural evidence of separation by liquid immiscibility of a granitic phase from mafic residual melt, primarily in the form of rounded, smooth-edged segregations of ovoid silica-potassium-feldspar granophyre (Figs. 1 and 2), set in the otherwise mafic assemblage (mainly pyroxene + plagioclase + phosphate). Other lunar samples containing similar assemblages exist, notably 15405 (Ryder 1976) and particles from 15403 (Marvin et al. 1990), and in sample

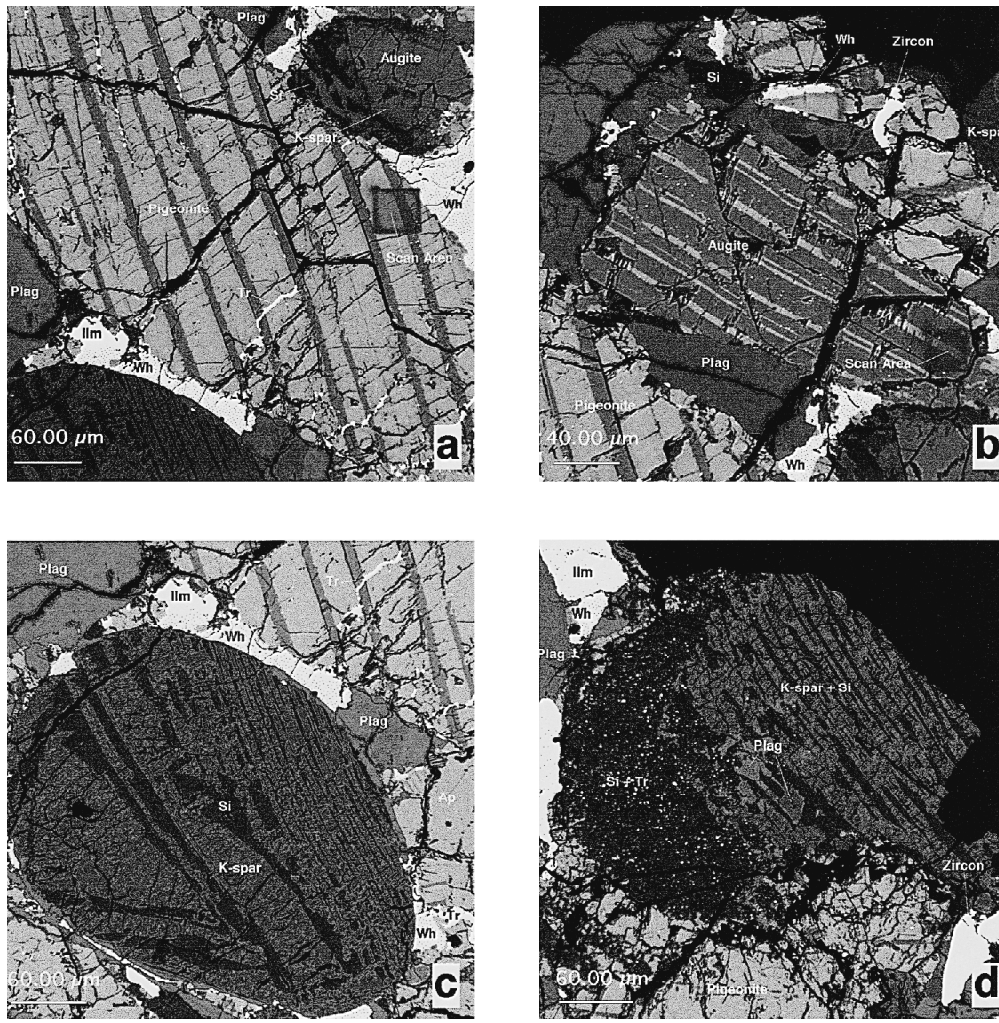

FIGURE 2. (a) BSE image of pigeonite with (001) augite lamellae. The pyroxenes show multiple fractures, some of which contain veins of troilite + silica + minor ilmenite. Some fractures are unfilled. Note the ovoid in right center containing silica + potassium feldspar and an augite grain surrounded by whitlockite. The darker square labeled "scan area" outlines the areas that were scanned by EMPA for the profile measurements. Note that exsolution lamellae extend to the grain edge with no change in thickness, e.g., just above the scan area in pigeonite. **(b)** BSE image of fractured augite with (001) pigeonite lamellae. The darker square outlines the area that was scanned for profile measurement. **(c)** BSE image of egg-shaped segregation of granophyre containing silica and potassium feldspar. Note the minerals (whitlockite, plagioclase, apatite, ilmenite) molded around the exterior of the granophyre. **(d)** BSE image of a broken granophyric segregation adjacent to silica containing disseminated, very fine-grained blebs of troilite, interpreted to have exsolved late from siliceous melt.

12013, Quick et al. (1977) observed ovoid blebs of felsite in a mafic groundmass and interpreted them as products of SLI. However, no other lunar samples have similarly coarse pyroxene exsolution and textures that so clearly indicate SLI. Previously, we used ion and electron microprobes to determine the compositions and the distribution of REE between the phosphate minerals apatite and whitlockite in 14161,7373 (Jolliff et al. 1993). The following description summarizes previous observations as well as some new ones.

The dominant pyroxene is pigeonite, which contains augite lamellae up to 10 μm wide exsolved mainly on (001) of the host pigeonite (Fig. 2a). Augite hosts with pigeonite exsolution lamellae up to 5 μm wide on (001) are less abundant (Fig. 2b). Very fine shock-induced microstructures (lamellae, fractures) occur subparallel to (100) in some pyroxene grains, which Jolliff (1991) described as indicating incipient inversion; however, no high-Ca lamellae in pigeonite and no low-Ca lamellae in augite are observed parallel to (100) in high-magnification backscattered-electron (BSE) images. Also, the edges of lamellae, where not disrupted or offset by fractures, remain straight and parallel. In fact, the lamellae of augite in pigeonite and pigeonite in augite typically extend to the edge of the host grains with no change in thickness even when the grain boundary cuts across the lamellae at a high angle (Fig. 2a). This appears to be the case regardless of the mineral adjacent to the pyroxene. The simplest interpretation of this observation is that these pyroxene grains have suffered some post-exsolution abrasion or dissolution, possibly resulting from impact disruption, because in rocks with single

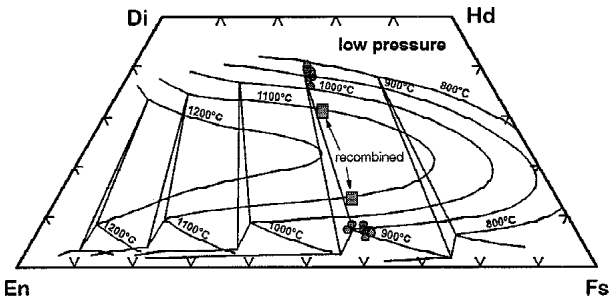

FIGURE 3. Pyroxene compositions in 14161,7373. Bulk compositions are shown by squares, host—lamellae pairs are shown as circles. Solvus isotherms at 800 °C, 900 °C, 1000 °C, 1100 °C, and 1200 °C after Sack and Ghiorso (1994) are projected onto the quadrilateral.

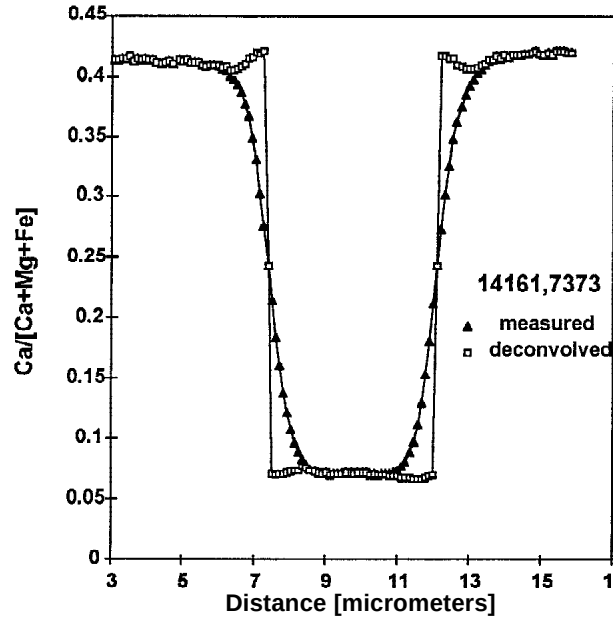

FIGURE 4. Measured profile and the deconvolved profile—note that beyond a distance of ~2 μm on either side of the interface, the measured and deconvolved profiles are identical as would be expected if the diameter of the excitation volume is less th–an ~4 μm. Note the minimum in the Ca/(Ca+Fe+Mg) of the host augite about 1 μm from the interface.

stage crystallization/cooling histories, exsolution lamellae taper markedly at pyroxene grain boundaries as the material closest to the grain boundary exsolves completely.

Pigeonite and augite grains contain fracture fillings consisting of stringers of troilite, ilmenite blebs, and silica (Figs. 1 and 2a). These post-exsolution veins appear to be restricted to the pyroxene and whitlockite grains, and are absent in the other minerals, suggesting that this rock has had a complex multi-stage history despite its overall igneous-like texture. All grains in this assemblage are fractured, and small offsets of exsolution lamellae in pyroxene grains are prominent. Many fractures are unfilled, suggesting that the healed fractures represent an early set.

In exsolved pyroxene grains, bulk compositions were calculated by integrating the host and lamellae compositions in the appropriate proportions as determined by analysis of BSE images of the grains. The bulk compositions are quite uniform [bulk pigeonite composition: $En_{34.4}$ $Fs_{51.2}Wo_{14.4}$; bulk augite composition: $En_{30.2}Fs_{36.7}Wo_{33.2}$]. The host and lamellae components are also quite uniform [pigeonite host: $En_{36.1}Fs_{57.3}Wo_{6.6}$; augite lamellae: $En_{28.8}Fs_{30.6}Wo_{40.6}$; augite host: $En_{28.6}Fs_{29.4}Wo_{42}$; pigeonite lamellae: $En_{34.8}Fs_{58.4}Wo_{6.8}$]. Compositions of a typical coexisting pair and their exsolved components are plotted in Figure 3. Using the Sack and Ghiorso (1994) solvus, the equilibration temperature for the bulk pigeonite-augite pairs is about 1100 °C. The host-lamellae pairs indicate a closure temperature around 875–900 °C.

Plagioclase grains retain some compositional variation, ranging from coarse calcic grains ($An_{82}Ab_{17}Or_1$) to fine, interstitial, more sodic grains ($An_{57}Ab_{40}Or_3$). Zoning patterns are irregular and this may reflect, in part, grains that have undergone several episodes of crystallization and dissolution. Plagioclase grains are fractured and exhibit undulose extinction, but were not converted to maskelynite by impact. The margins of some plagioclase grains enclose small potassium feldspar grains plus silica, but plagioclase grains, in general, are free of troilite veins. Potassium feldspar (average $Or_{83}Ab_{12}Cn_{3.5}An_{1.7}$ and containing up to 2.25 wt% BaO) occurs as discrete grains up to 100 μm and as granophyric intergrowths with silica in smooth-edged, ovoid-shaped masses, the largest of which is 400 × 250 μm (Fig. 2c). The shape of the ovoids and their internal textures are strongly suggestive of SLI.

Silica is present in several forms, identified by laser Raman spectroscopy: amorphous silica grains, containing very fine-grained patches of quartz, and some "relict" cristobalite, with a characteristic hackle or tile-like fracture pattern. Silica also occurs as discrete grains and in granophyric intergrowths with potassium feldspar. In an unusual texture, several separate grains of silica contain abundant, disseminated troilite blebs (Fig. 2d) amounting to 2–3 wt% S.

The phosphates, whitlockite and apatite, both occur in this assemblage, although the proportion of whitlockite greatly exceeds that of apatite. Whitlockite grains are REE-rich, but are not as enriched as in some other lunar samples (Jolliff et al. 1993). Whitlockite grains range in size from over 500 μm to fine interstitial grains; the latter are commonly molded around the curved exterior of the granophyre ovoids (Fig. 2c). Anhedral, equant fluorapatite grains containing 0.7–0.9 wt% Cl and ranging up to 100 μm in grain size occur interstitially, typically associated with whitlockite.

Accessory minerals in the assemblage include ilmenite, zircon, and troilite. Ilmenite forms anhedral to blocky grains, and constitutes only about 2 vol% of the sample (Fig. 1). The thin section reveals only a few small zircon grains (Figs. 2b and 2d), but the bulk concentration of Zr (7150 ppm) indicates as much as 1 vol% in the original "whole-rock" sample. Troilite is present as discrete, small grains, as fracture fillings, and as minute blebs within silica grains (Fig. 2d).

METHODOLOGY

Profile measurement in pyroxene

Major and minor elements in pyroxene grains used for profile measurements were analyzed using a JEOL 733 Superprobe at the University of Washington (Seattle). All analyses were done

using an accelerating voltage of 15 kV. ZAF corrections were applied to all analyses. Compositional profiles were measured across host-(001) lamellae pairs in augites and uninverted pigeonite crystals in which the (001) lamellae are oriented perpendicular to the surface of the section. For pyroxene grains with lamellae widths <5 mm, conventional step scanning at 1 μm intervals provides an inadequate number of data points to reveal the details of compositional variations. To address the problem of too few data points, we adopted a beam-scanning technique in which an area encompassing a host-lamella pair was scanned and X-ray counts corresponding to Ca, Mg, Fe, and Al were collected during scanning. The pixel size varied depending on the area scanned, e.g., an area of 20 × 20 μm has pixels of 0.045 μm. Counting times up to 24 h were required to obtain a statistically meaningful number of counts per pixel. Areas scanned in pigeonite and augite appear in Figures 2a and 2b as darkened squares. Appropriate profiles (parallel to *c*) were selected from the infinite number of possible profiles. Counts were converted to wt% oxide using correction factors obtained from conventional probe analysis of individual host and lamellae. This method does not, of course, improve resolution but it does provide a much larger set of compositional data, which greatly improves deconvolution calculations.

In addition to the standard microprobe correction procedures, it is essential to correct the data for overlap effects in the vicinity of lamellae-host interfaces because the measured composition represents a weighted average of the volume of sample excited by the electron beam (Ganguly et al. 1988). The magnitude of the overlap effect is different for each element and is primarily a function of the excitation voltage. The volume of excitation around the incident beam is assumed to have a radially symmetric Gaussian intensity distribution with a standard deviation (ε) that can be calculated from the slope of the measured profile at the interface (see Ganguly et al. 1988, p. 903). For Ca, for example, ε has a value of 0.55. Because deconvolution is extremely difficult to do, we follow the method of Ganguly et al. (1988) in which a hypothetical concentration profile is convolved and the correction factors obtained from this convolution are applied to the measured profile. In practice, it is usually only necessary to correct the raw data for a distance of a few micrometers on either side of the interface. However, as shown in Figure 4, in which a measured and deconvolved profile are compared, the effect of the spatial averaging is significant and attempts to model profiles without first deconvolving them are subject to large errors.

Computation of cooling rates

An estimate of the closure temperature (the temperature below which interdiffusion of Ca, Fe, and Mg on the submicrometer scale is insignificant) is made from the compositions of host and lamellae pairs. The compositions are plotted on the Sack and Ghiorso (1994) phase diagram, which shows isotherms at 100°C intervals from 1200 to 800 °C on the pyroxene solvus as a function of composition (Fig. 3). Because most of the host-lamellae data plot between the 800 and 900 °C isotherm, it was assumed that diffusion on the scale resolvable by microprobe analysis was ineffective below ~850 °C.

The (001) lamellae in augite and pigeonite grow along a planar front by interdiffusion of Ca and Mg,Fe parallel to the *c* axis; thus a one-dimensional solution to the diffusion equation is sufficient. To simulate lamellae growth, we used a numerical solution to the diffusion equation that allows for compositional and temperature-dependent diffusion coefficients. A discussion of the appropriate equations, diffusion coefficients used, and computational method is given in McCallum and O'Brien (1996). Both linear and exponential cooling rate functions were used; there was very little difference in the calculated profiles.

An accurate representation of the pyroxene solvus is required. We have used the solvus parameters determined recently by Sack and Ghiorso (1994). For the particular composition being modeled, a section through the solvus at the appropriate Mg/(Mg+Fe) value was computed. The correct solvus and tie lines are critical in the calculations since these determine the temperature of initiation of exsolution, the extent of exsolution, and the compositions of the host and lamellae as a function of temperature.

In the simulation of compositional profiles, it is necessary to specify an appropriate field length for diffusion. In practice, this is taken as the half-width of a lamella plus the half-width of an adjacent host as measured on the crystal whose profile is being simulated. Additional input parameters are bulk Ca/(Ca+Mg+Fe) and Fe/(Mg+Fe) of the pyroxene, and the closure temperature for diffusion.

TABLE 1. REE concentrations (ppm) in pyroxene in 14161,7373

	Pig 1	Pig 2	Pig 3	Aug 1	Aug 2	Aug 3
Y	58.0 ± 1.2	36.6 ± 1.4	26.9 ± 0.9	155.3 ± 3.1	151.5 ± 3.1	114.7 ± 3.6
La	0.56 ± 0.08	0.53 ± 0.07	0.43 ± 0.08	3.17 ± 0.41	3.09 ± 0.41	4.23 ± 0.60
Ce	1.99 ± 0.20	1.26 ± 0.17	1.24 ± 0.17	12.5 ± 1.1	13.5 ± 1.1	19.2 ± 1.7
Pr	0.42 ± 0.05	0.22 ± 0.04	0.22 ± 0.03	2.89 ± 0.40	2.81 ± 0.33	4.34 ± 0.48
Nd	2.48 ± 0.17	1.23 ± 0.13	1.14 ± 0.11	14.8 ± 1.0	18.1 ± 1.5	20.3 ± 1.3
Sm	1.51 ± 0.11	0.66 ± 0.09	0.61 ± 0.07	8.30 ± 0.65	8.87 ± 0.83	8.10 ± 0.81
Eu	0.030± 0.014	0.017± 0.015	0.008± 0.010	0.20 ± 0.08	0.29 ± 0.08	0.11 ± 0.22
Gd	2.2 ± 0.4	1.3 ± 0.3	0.8 ± 0.2	10.3 ± 1.6	9.6 ± 1.7	7.7 ± 1.5
Tb	0.75 ± 0.10	0.46 ± 0.08	0.29 ± 0.06	2.99 ± 0.36	2.38 ± 0.43	2.34 ± 0.43
Dy	7.20 ± 0.47	4.48 ± 0.39	3.18 ± 0.27	23.6 ± 1.5	23.3 ± 1.6	17.7 ± 1.2
Ho	1.88 ± 0.19	1.22 ± 0.16	0.95 ± 0.18	5.22 ± 0.50	4.96 ± 0.66	4.41 ± 0.47
Er	7.01 ± 0.46	5.10 ± 0.35	3.71 ± 0.27	17.2 ± 1.1	16.6 ± 1.3	11.5 ± 0.9
Tm	1.06 ± 0.17	0.96 ± 0.11	0.76 ± 0.07	2.85 ± 0.33	2.48 ± 0.40	2.00 ± 0.22
Yb	12.6 ± 0.8	8.1 ± 0.7	6.5 ± 0.5	21.8 ± 1.5	20.1 ± 1.7	19.4 ± 1.6
Lu	1.91 ± 0.27	1.46 ± 0.24	1.20 ± 0.15	3.29 ± 0.49	3.35 ± 0.43	2.05 ± 0.38

Notes: Pig 1 = coarse grain 1 (~450 μm), pigeonite host; Pig 2 = coarse grain 2 (~300 μm), near edge of grain; Pig 3 = coarse grain 3 (~500 μm), between center of grain and edge, in an area lacking exsolution lamellae; Aug 1 = augite lamella, coarse grain 1 (cf. Pig 1), slight (<10%) overlap onto pigeonite host; Aug 2 = medium grain (~250 μm), exsolved, augite host, overlap onto pigeonite lamellae (~22%); Aug 3 = small (~100 μm), interstitial grain; no pigeonite lamellae; intergrown with silica, plagioclase, and potassium feldspar. Uncertainties are 1σ, based on counting statistics.

TABLE 2. REE concentrations (ppm) in feldspars in 14161,7373

	Plg 1	Plg 2a	Plg 2b	Plg 3	Kfs 1	Kfs 2
Y	1.73 ± 0.07	2.41 ± 0.18	2.80 ± 0.16	1.39 ± 0.11	0.43 ± 0.06	0.84 ± 0.13
La	4.79 ± 0.20	4.97 ± 0.34	6.12 ± 0.24	3.33 ± 0.22	1.35 ± 0.11	1.87 ± 0.18
Ce	9.01 ± 0.24	9.59 ± 0.45	11.8 ± 0.4	5.31 ± 0.40	0.45 ± 0.06	1.50 ± 0.20
Pr	0.90 ± 0.05	0.82 ± 0.06	1.11 ± 0.07	0.48 ± 0.05	0.04 ± 0.01	0.11 ± 0.03
Nd	2.94 ± 0.09	3.39 ± 0.16	4.18 ± 0.16	1.69 ± 0.09	0.16 ± 0.03	0.51 ± 0.09
Sm	0.38 ± 0.03	0.36 ± 0.06	0.52 ± 0.05	0.15 ± 0.04	ui	ui
Eu	3.40 ± 0.13	3.29 ± 0.16	3.29 ± 0.12	3.71 ± 0.26	ui	ui
Gd	0.36 ± 0.06	0.48 ± 0.11	0.57 ± 0.09	0.23 ± 0.06	bd	bd
Tb	0.07 ± 0.01	0.08 ± 0.02	0.08 ± 0.01	0.04 ± 0.01	ui	ui
Dy	0.38 ± 0.02	0.45 ± 0.04	0.50 ± 0.04	0.24 ± 0.03	ui	ui
Ho	0.07 ± 0.01	0.09 ± 0.01	0.09 ± 0.01	0.07 ± 0.01	ui	ui
Er	0.17 ± 0.02	0.30 ± 0.03	0.26 ± 0.03	0.27 ± 0.04	ui	ui
Tm	0.03 ± 0.02	0.02 ± 0.02	0.03 ± 0.01	0.02 ± 0.02	ui	ui
*Yb	0.23 ± 0.02	0.52 ± 0.06	0.15 ± 0.02	0.17 ± 0.03	0.43 ± 0.02	0.85 ± 0.02
Lu	0.020± 0.005	0.019± 0.010	0.017± 0.007	0.014± 0.009	ui	ui

Notes: Plg 1 = 600 × 275 µm grain size; Plg 2a = 300 × 180 µm, center of grain; Plg 2b = 300 × 180 µm, sodic patch at one end of the grain; Plg 3 = 200 × 80 µm. Kfs 1 = in granophyric intergrowth; and Kfs 2 = 75 ×150 µm separate grain. Uncertainties are 1σ, based on counting statistics. ui = unresolved interference; bd = below detection.
*Concentrations of Yb are considered to be upper limits because of interferences caused by neutron irradiation (see text).

Sources of error are (1) analytical uncertainty (~±2 % relative), (2) width and spacing of host and lamellae (±1 % relative), (3) solvus parameters (~±2 % relative), (4) deconvolution calculations, and (5) diffusion coefficients. The deconvolution calculations are based on the slope of the measured profile at the interface (Fig. 4), which can be determined accurately. The diffusion coefficients represent the major source of uncertainty in the computation of cooling rates because measured values of $D_{Ca\text{-}FeMg}$ extend only to 1000 °C and a significant fraction of lamellar growth occurs below 1000 °C. We used a linear extrapolation on a log D vs. 1/T plot to estimate diffusion coefficients below 1000 °C. The interdiffusion of Ca and Fe+Mg in pyroxene is most likely also dependent on Mg/(Mg+Fe), but there are insufficient data to assess this effect (Ganguly and Tazzoli, 1994). From the data of K. Fujino (personal communication), the errors in the measured diffusion coefficients are estimated at ±0.3 log units between 1200 and 1100 °C and ±0.35 log units between 1100 and 1000 °C. The uncertainty in the diffusion coefficients propagates to the same uncertainty in the cooling rate. We estimate the overall uncertainty in the calculated cooling rates to be approximately ±0.5 log unit and certainly less than ±1.0 log unit.

Cooling rate and depth of burial

Several factors control cooling rates, and it is not possible to specify a unique depth of burial corresponding to a given cooling rate. Primary factors controlling the cooling rate include the size and shape of the magma body, the location of a sample within the body, the thermal diffusivities of the magma, its crystalline equivalent, and the surrounding country rock, thickness of country rock cover, temperature and temperature gradients in country rock and magma, and processes such as convection, crystal accumulation, and assimilation in the magma chamber. The most relevant treatments of cooling in plutonic mafic systems are those of Jaeger (1968) and Irvine (1970), and we have adopted models discussed in these papers.

Additional complications in the case of the Moon arise as a consequence of the extensive brecciation of lunar crustal rocks early in lunar history and the development of a megaregolith. Thermal diffusivities of brecciated and porous samples can be an order of magnitude (or more) lower than those of coherent rocks of the same composition. In our calculations to place constraints on the depth of burial of lunar samples, we assume a value for the thermal conductivity of the megaregolith of 0.2 W/m·deg (Warren et al. 1991) and a value of 1.5 W/m·deg for molten and crystalline lunar gabbro/basalt (Horai and Winkler 1976).

Ion probe measurements

The concentrations of REE and other trace elements were measured using a modified Cameca 3-f ion microprobe according to methods given by Zinner and Crozaz (1986). Details of the experimental procedure are given by Floss et al. (1990). Sensitivity factors for the REE in pyroxene were determined from synthetic glass standards (Drake and Weill 1972), and sensitivity factors for the REE in plagioclase were obtained by comparing ion-microprobe analyses to INA analyses of coarse lunar anorthite grains (Floss and Jolliff 1997). These give results for analyses of plagioclase from a variety of lunar ferroan anorthosites (Jolliff and Hsu 1996; Floss et al. 1998) that are in agreement with REE concentrations measured by INAA. All measurements were normalized using Si as the reference element; SiO_2 concentrations were determined by electron microprobe analyses of the same grains analyzed with the ion microprobe. Electron-microprobe analyses supporting the ion-microprobe analyses were made with the JEOL 733 Superprobe at Washington University (St. Louis) using an accelerating voltage of 15 kV, natural mineral standards, and ZAF correction procedures. Table 1 lists the REE concentrations in pyroxene, Table 2 lists the REE concentrations in feldspar, and Table 3 lists the corresponding major-element compositions.

Prior to preparation of the thin section used for ion microprobe analysis, sample 14161,7373 was irradiated for INAA (Jolliff 1991). Several of the REE measured with the ion microprobe have large cross sections for the absorption of thermal neutrons, namely ^{149}Sm, ^{155}Gd, ^{156}Gd, and ^{151}Eu. The reactions of concern are $^{149}Sm(n,\gamma)^{150}Sm$, $^{155}Gd(n,\gamma)^{156}Gd$, $^{157}Gd(n,\gamma)^{158}Gd$, and in the case of plagioclase, $^{151}Eu(n,\gamma)^{152}Eu$, which has three isomeric states leading to stable ^{152}Eu, ^{152}Sm, and ^{152}Gd. From the thermal neutron flux and irradiation duration, we calculated the post-irradiation isotopic abundances of

TABLE 3. Major-element compositions of pyroxene and plagioclase corresponding to ion-microprobe analysis spots, 14161,7373.

	Pyroxene					
	Pig 1	Pig 2	Pig 3	Aug 1	Aug 2	Aug 3
SiO_2	49.1	49.6	50.5	49.5	50.2	49.6
TiO_2	0.24	0.24	0.23	0.76	0.58	0.66
Al_2O_3	0.40	0.45	0.25	1.21	0.97	2.58
Cr_2O_3	0.21	0.17	0.08	0.34	0.34	0.92
FeO	33.8	33.4	34.6	18.1	21.6	17.7
MnO	0.52	0.57	0.57	0.28	0.31	0.25
MgO	12.4	12.1	12.3	10.3	10.4	9.45
CaO	3.57	3.90	3.28	18.7	15.6	18.7
Na_2O	0.03	0.02	0.01	0.13	0.08	0.13
Sum	100.3	100.4	101.9	99.3	100.1	99.9
En	36.5	36.0	36.1	30.3	30.7	28.8
Fs	56.0	55.6	57.0	30.0	36.0	30.2
Wo	7.6	8.3	6.9	39.8	33.3	41.0
Mg/(Mg+Fe)	0.39	0.39	0.39	0.50	0.46	0.49
	Plagioclase					
	Plg 1	Plg 2a	Plg 2b	Plg 3	Kfs 1	Kfs 2
SiO_2	47.7	47.7	48.2	52.5	62.7	62.6
Al_2O_3	33.3	33.4	33.4	29.9	18.8	19.0
FeO	0.14	0.20	0.19	0.43	0.07	0.13
MgO	0.02	0.02	0.02	0.03	<0.01	<0.01
CaO	16.8	16.4	15.9	12.5	0.26	0.34
BaO	nd	nd	nd	nd	1.75	1.90
Na_2O	1.94	2.13	2.34	4.01	1.27	1.30
K_2O	0.18	0.17	0.18	0.43	14.2	14.1
Sum	100.0	100.0	100.1	99.8	99.1	99.4
An	81.9	80.2	78.1	61.7	1.3	1.7
Ab	17.1	18.8	20.8	35.8	11.4	11.7
Or	1.0	1.0	1.1	2.5	84.1	83.2
Cn	nd	nd	nd	nd	3.2	3.4

Notes: En = enstatite, Fs = ferrosilite, Wo = wollastonite, An = anorthite, Ab = albite, Or = orthoclase, Cn = celsian, nd = not determined. Pyroxene and feldspar end-members calculated from atomic proportions on the basis of six O atoms (pyroxene) and eight O atoms (feldspar). Mg/(Mg+Fe) calculated from cation proportions, all Fe taken as Fe^{2+}.

these isotopes for use in our program for deconvolving the REE mass spectrum. We also used the post-irradiation isotopic ratios to correct the affected REE monoxides that might interfere with measured masses of the HREE. Despite this correction, we still observe some anomalies, especially for Gd and Yb, that appear to be related to neutron irradiation (e.g., low Gd and high Yb.) These anomalies vary from spot to spot, indicating that they may be related to local variations in the neutron flux, resulting from the high abundance of whitlockite, which is rich in Gd and other REE that have high neutron-capture cross sections. In all of our plots, REE concentrations are normalized to those in chondritic meteorites as given by Anders and Grevesse (1989) times a factor of 1.36, which gives a value of Sm = 0.2000 for consistency with our previously published INAA results (e.g., Jolliff et al. 1991).

RESULTS

Cooling rate models

We have modeled the exsolution process in both pigeonite and augite. The augite data are preferable because the host augite and (001) pigeonite lamellae were oriented normal to the surface. Consequently, the measured profiles are symmetrical. In the pigeonite, the measured profiles were slightly asymmetrical indicating that the lamellae in the measured grain were not perfectly normal to the surface. Figure 4 shows the measured profile and the deconvolved profile; note that beyond a distance of

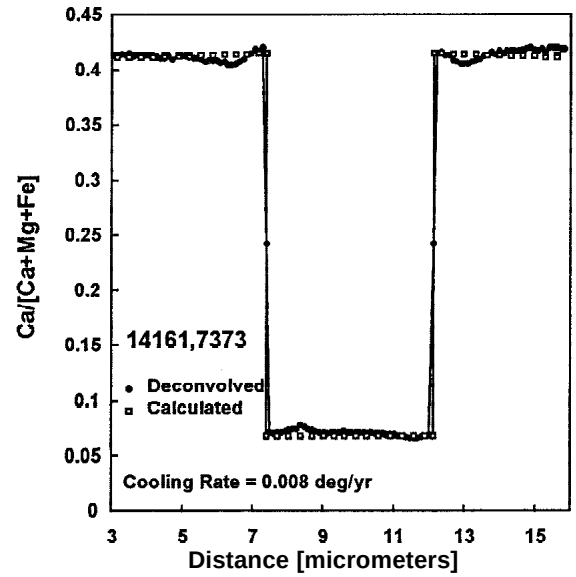

FIGURE 5. Calculated profile, based on a cooling rate of 8×10^{-3} deg/y, superimposed on the deconvolved profile. It is impossible to calculate a profile using a single monotonic cooling rate that simultaneously fits the main part of the profile and the compositional variations in the vicinity of the interface.

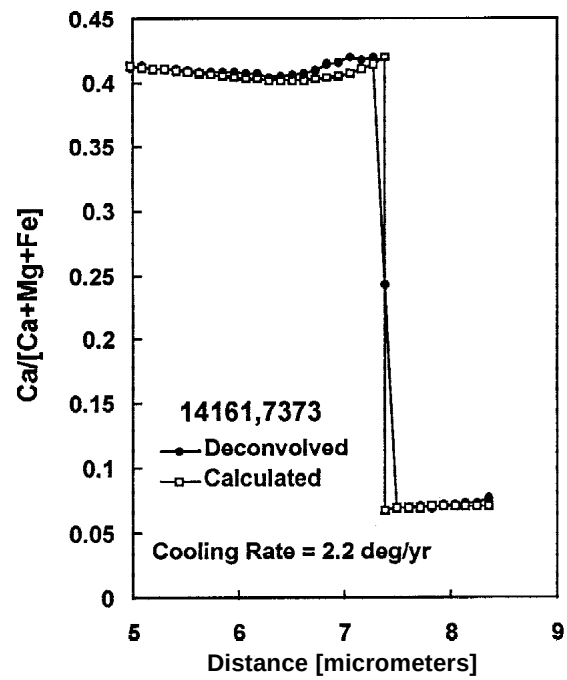

FIGURE 6. Calculated profile superimposed on the deconvolved profile in the vicinity of the host—lamella interface. The calculated profile is based on a reheating of the pyroxene to 980 °C followed by a period of rapid cooling to the closure temperature (~850 °C). The best-fit cooling rate is 2.2 °C/y, which corresponds to a depth of burial of ~30 meters.

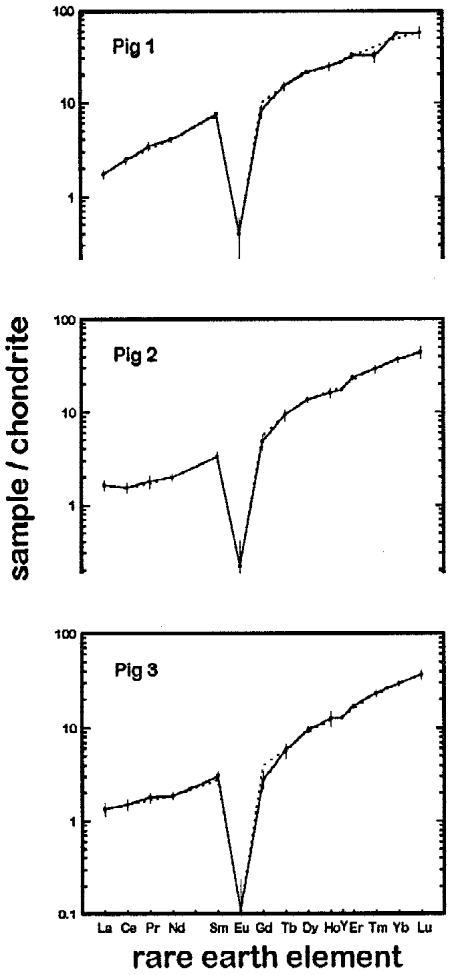

FIGURE 7. REE concentrations in pigeonite in 14161,7373, normalized to chondrites (see Table 1). Error bars are based on counting statistics (1σ). Y is plotted between Ho and Er. Anomalous values for Gd (typically low) and Yb (typically high) are attributed to effects of neutron irradiation of the sample (see text). The dashed lines represent smoothed values used for plotting in Figure 11. All three spot analyses are from coarse, exsolved grains (e.g., Fig. 2a) and represent the REE concentrations of the pigeonite hosts.

~2 μm on either side of the interface, the measured and deconvolved profiles are identical as one would expect if the diameter of the excitation volume is less than ~4 μm. As modeled, a minimum in the deconvolved profile of Ca/(Ca+Fe+Mg) of the host augite occurs about 1 μm from the interface.

Figure 5 shows the calculated profile, based on a cooling rate of 8×10^{-3} deg/year over the temperature interval from 1105 to 825 °C, superimposed on the deconvolved profile. The calculated profile provides a good fit to the lamella width and the measured profile a few micrometers removed from the interface, and this cooling rate is appropriate for the initial stage of exsolution. However, it does not provide a good fit to the measured (deconvolved) profile close to the interface. It is impossible to calculate a profile using a single stage cooling that simultaneously fits the main part of the profile and the compositional variations in the vicinity of the interface.

With increasing distance from the interface, the measured (deconvolved) profile first shows a decrease in Ca/(Ca+Fe+Mg) in augite from 0.42 to 0.405, then a minimum at a distance of 0.98 μm followed by an increase until Ca/(Ca+Fe+Mg) reaches a constant value of 0.413 (Fig. 5). To reproduce this profile, it is necessary to reheat the pyroxene (from some temperature below the closure temperature) for a short period of time to a temperature of 980 ± 30 °C followed by a period of rapid cooling to the second-stage closure temperature (850 °C). The short-lived reheating results in a profile in which the augite host shows a gradient of decreasing Ca/(Ca+Fe+Mg) toward the interface while the pigeonite lamella shows the opposite gradient as the two components try to reach a composition corresponding to equilibrium at 980 °C. The effect in the pigeonite lamella is much less pronounced because the interdiffusion of Ca and Fe+Mg in pigeonite is an order of magnitude more rapid (McCallum and O'Brien 1996). During the subsequent (second stage) cooling, the pyroxene reestablishes a characteristic diffusion gradient close to the interface. The cooling rate that gives the best fit is 2.2 °C/year (Fig. 6). Although the fit is not perfect, the cooling rate is tightly constrained by the location of the minimum in the deconvolved profile.

As pointed out above, it is not possible to establish a unique depth from cooling rates. However, several of conclusions can be reached vis-a-vis the thermal history of sample 14161. (1) The slow cooling during the first stage (0.008 °C/year) is incompatible with any lava flow or lava pond because such a pond would have to be in excess of 2 km thick. (2) Assuming that the sample crystallized in a sill-like intrusion, a cover thickness of only 500 m of megaregolith material has the same effect as an infinitely thick cover due to the very low thermal conductivity of this material. (3) A sill-like intrusion overlain by ≥500 m of megaregolith material would need to have a minimum thickness of ~1 km. All thinner sills cool too quickly regardless of location within the sill. (4) For any sill ≥1 km in thickness under a cover of 500 m, a sample cooling at the rate of 0.008 °C/year must be located a *minimum* depth below the surface of 750–800 m. (5) The second stage reheating/recooling is consistent with a burial depth of 30 m in an ejecta blanket, regardless of the thickness of the blanket.

Ion microprobe results

In coarsely exsolved pigeonite, we analyzed the low-Ca host of three different grains, as well as an augite lamella (Aug 1 and Pig 1 are adjacent analyses from the same grain). We also analyzed a separate, exsolved augite grain as well as a small homogeneous augite grain. Concentrations of the REE in the pigeonite and augite are given in Table 1 and plotted in Figures 7 and 8. We analyzed a coarse, relatively calcic plagioclase grain (An_{82}), a smaller grain (An_{80}) that has a relatively sodic area on one end (An_{78}), and a smaller, more albitic interstitial grain (An_{60}). Two analyses were made of potassium feldspar, one within a granophyric intergrowth (Fig. 2c) and one of a separate grain. Concentrations of the REE in plagioclase and potassium feldspar are given in Table 2 and plotted in Figures 9 and 10. The potassium feldspar grains have very low REE concentrations and, because of interferences from Ba monoxides, we could reliably measure only the LREE, Y, and Yb.

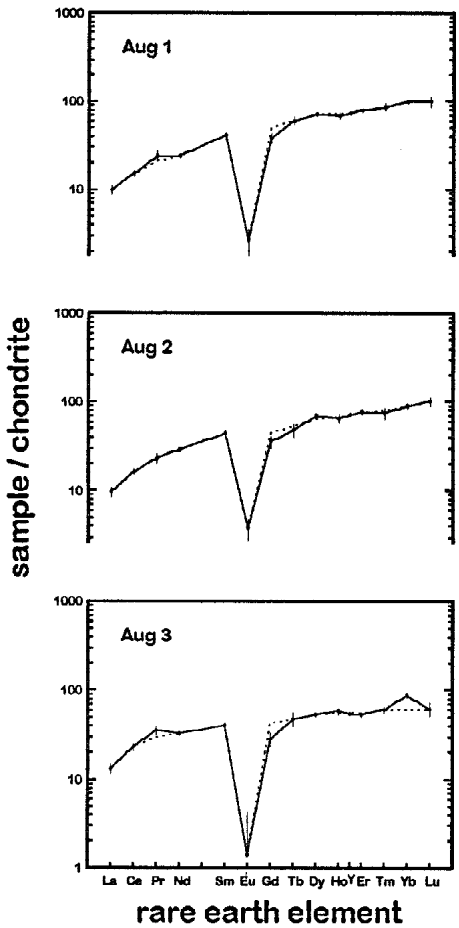

FIGURE 8. REE concentrations in augite in 14161,7373, normalized to chondrites (see Table 1). Anomalous values for Gd (typically low) and Yb (typically high - pronounced for Aug 3) are attributed to effects of neutron irradiation of the sample (see text). The dashed lines represent smoothed values used for plotting in subsequent figures (Fig. 11). Aug 1 represents the composition of a single augite lamella in the same grain as (and adjacent to) Pig 1. Aug 2 (Fig. 2b) represents the composition of the augite host of an exsolved augite grain, but contains an estimated 20% overlap (based on Ca content) onto pigeonite lamellae. Aug 3 is from a small, interstitial grain that contains no visible pigeonite exsolution lamellae (small ovoid, upper right of Fig 2a).

Among the analyzed silicates, augite has the highest trivalent REE concentrations (Fig. 11). Two of the augite spots, Aug 1 (a thick lamella in coarse pigeonite) and Aug 2 (augite host in an exsolved augite grain), yielded similar REE concentrations, but the third, Aug 3, has a distinctly flatter LREE/HREE slope (Fig. 11). Aug 3 is a small (~100 µm) grain that occurs in an elliptical intergrowth with plagioclase, silica, and potassium feldspar (Fig. 2a). Concentrations of REE in pigeonite are lower than those in augite. The differences are generally consistent with different partitioning between the two types of pyroxene (e.g., McKay et al. 1986; Papike et al. 1996); however, augite/pigeonite REE values in 14161,7373 are significantly lower than experimental partition coefficients and other natural augite-pigeonite pairs by factors of ~3–10 for the LREE and ~2 for the HREE (see discussion).

Concentrations of the REE in the three pigeonite spots, all from coarse, exsolved grains, vary by about a factor of two (Table 1) despite the fact that major-element compositions are uniform. We avoided exsolution lamellae with the ion microprobe, and Ca data from the ion microprobe verify this. By comparison to the variations in REE concentration in plagioclase (see below), we interpret the range of concentrations in pigeonite as an early (high concentration) to late (low concentration) crystallization sequence. This sequence is consistent with variations in Ti/(Ti+Cr) (mainly Cr), wherein the analysis we take to represent earliest formed pigeonite (Pig 1) has the lowest Ti/(Ti+Cr). The REE pattern for the grain with the lowest REE concentrations (Pig 3) is slightly depleted in the middle REE (MREE), which is also the case for plagioclase (Fig. 11). With only three spot analyses of REE in pigeonite, we cannot say whether these variations represent distinct generations, or simply random samples in a continuous sequence.

Plagioclase REE patterns have steep LREE slopes, relatively flat HREE slopes, and strongly positive Eu anomalies. REE concentrations span a range of about a factor of two, but in this case, REE variations correspond to variations in Na concentrations and grain size that provide clues to the crystallization sequence (Fig. 11b). The central spots (Plg 1, Plg 2a) of two large, relatively calcic, presumably early grains ($An_{80\text{-}82}$) have similar REE concentrations; however, the sodic end (An_{78}) of one of these grains (Plg 2b) has slightly higher REE concentrations (Fig. 11b). The small, interstitial, relatively sodic (An_{62}, presumably late) grain (Plg 3), on the other hand, has the lowest REE concentrations, particularly in the MREE.

Concentrations of REE in potassium feldspar are extremely low (Fig. 11b). One of the grains (Kfs 1) is from a granophyric intergrowth of silica and potassium feldspar (Fig. 2c). The other grain (Kfs 2) occurs as a separate, ~150 µm grain, not intergrown with silica. The REE concentrations of Kfs 1 are significantly lower than those of Kfs 2 and appear to be depleted most in the MREE.

DISCUSSION

The major-element compositions of pyroxene and plagioclase place sample 14161,7373 in the alkali suite of lunar intrusive rocks (Fig. 12). Although pyroxene major-element compositions are well equilibrated, plagioclase compositions range from about An_{80} to An_{60}, reflecting the relatively rapid exchange of Mg and Fe^{2+} in pyroxene compared to the sluggish exchange of NaSi for CaAl in plagioclase. Superimposed on Figure 12 is a field inferred for mineral compositional evolution during the crystallization of KREEP basalt and KREEPy impact-melt rocks (cf. Longhi 1989; Snyder et al. 1995), suggesting that the mineral compositions of 14161,7373 are consistent with a magnesian- or alkali-suite parentage, albeit toward the highly fractionated end of the series. The bulk composition of 14161,7373 is not that of a eutectic assemblage, as it is enriched in pyroxene and whitlockite compared to relevant cotectic or eutectic liquids (estimated using the computer parameterization of Longhi, e.g., Longhi 1991). However, the assemblage includes potassium feldspar and silica, in addition to plagioclase and two types of pyroxene, indicating that the equilib-

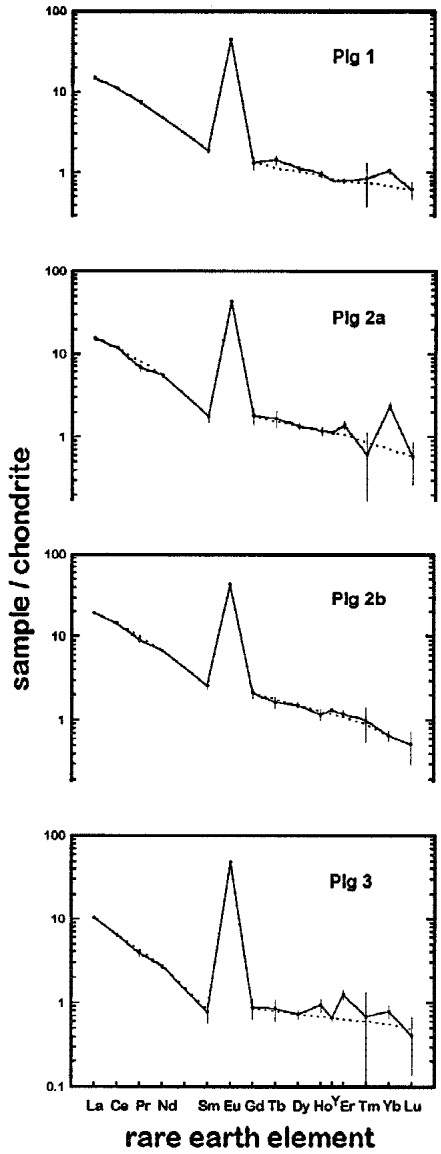

FIGURE 9. REE concentrations in plagioclase in 14161,7373, normalized to chondrites (see Table 2). Anomalous values for several of the HREE are attributed in part to effects of neutron irradiation of the sample and in part to interferences of the LREE monoxides at masses of HREE coupled with low HREE concentrations, which combine to give large uncertainties. The dashed lines represents smoothed values used for plotting in subsequent figures (Fig. 11). For the smoothed values, Y, plotted between Ho and Er, was weighted heavily in order to establish the HREE slope. Plg 1 is from the center of a coarse grain (Fig. 1, lower left; An_{82}). Plg 2a is from the center of a smaller grain (Fig. 1, lower left-center; An_{80}) and Plg 2b is from a more sodic end/edge of the same grain (An_{78}). Plg 3 is from a small, interstitial, more sodic grain (Fig. 1, near center; An_{62}).

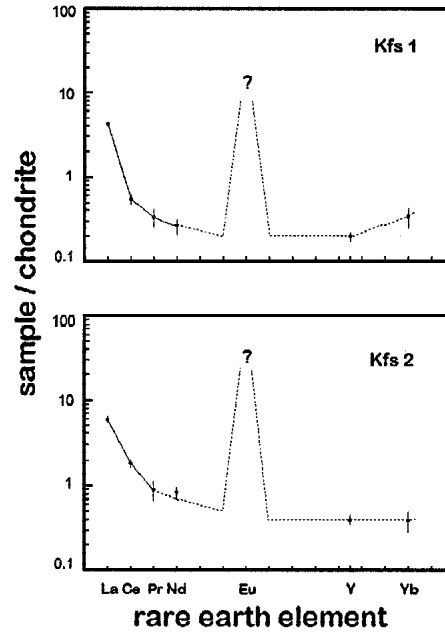

FIGURE 10. REE concentrations in potassium feldspar in 14161,7373, normalized to chondrites. The dashed line represents smoothed values used for plotting in Figure 11. Strong interferences from Ba oxides prevented the determination of concentrations for most of the REE beyond Nd. For the smoothed values, Y, plotted between Ho and Er, was used to establish the HREE slope. Kfs 1 is from potassium feldspar in granophyric intergrowth with silica (Fig. 2c) and Kfs 2 is from a separate grain, not intergrown with silica.

rium melt (and possibly the parent melt) for this sample had a eutectic composition. Thus, the bulk-rock composition reflects either an accumulation of pyroxene (and phosphate) and/or a loss of a felsic (granitic) component. We do not believe that the mode and bulk composition of this assemblage simply reflect non-representative sampling (due to small size) because the missing fraction has precisely the trace-element signature expected of a granitic residual melt (Jolliff 1991).

Equilibrium melt

Given that this sample retains relict igneous texture and appears to be monomict (Jolliff 1991; Warren 1993), it is tempting to use experimental mineral/melt partition coefficients coupled with REE concentrations of minerals to estimate REE concentrations in the melt that would have been in equilibrium with the silicates. This has been done for magnesian-suite cumulates by Papike et al. (1994, 1996), who found that orthopyroxene and plagioclase gave self-consistent results, indicating equilibrium-melt REE concentrations at the level of high-K KREEP and higher. This finding means that the REE-rich whitlockite found in the samples studied by Papike et al. and other similar ones (e.g., Jolliff et al. 1993) may have formed from the same equilibrium melts, and that processes such as infiltration metasomatism are not needed to explain the presence of REE-rich whitlockite. In the case of 14161,7373, it appears, from the major-element compositions of minerals and from the assemblage of minerals and their textures, that the silicates and whitlockite are indeed cogenetic. We know the REE concentrations of coarse whitlockite in this sample (Jolliff et al. 1993), and from the mineral/melt partition coefficients for whitlockite, we would expect an equilibrium melt from 2–4× high-K KREEP, depending on the proportion of whitlockite

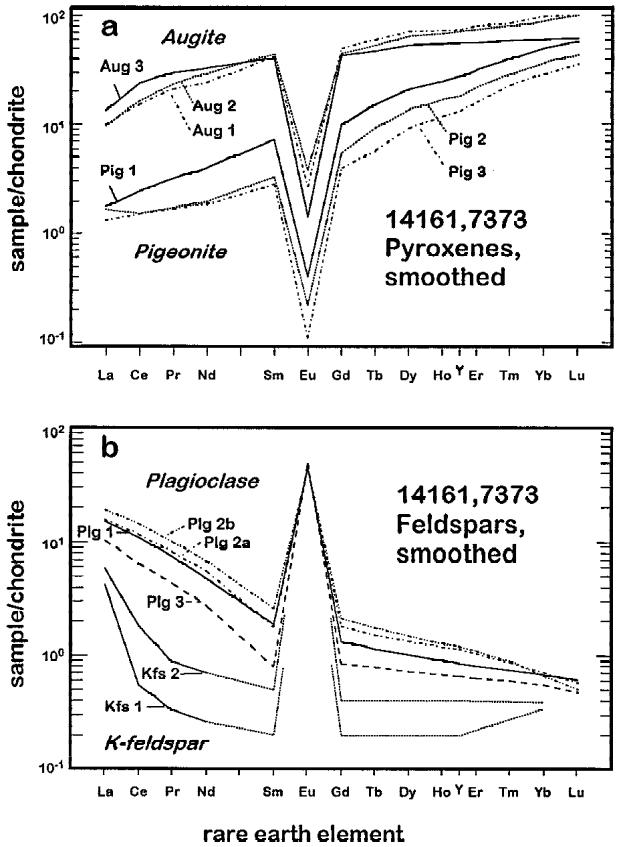

FIGURE 11. REE concentrations in pyroxene (a) and feldspar (b) in 14161,7373, smoothed patterns, normalized to chondrites. In (a) textural evidence indicates that Aug 3, which is fine-grained, interstitial, and contains no pigeonite exsolution lamellae, may have formed late relative to the others. In (b), the order of crystallization is inferred, based on grain size and An content, to be Plg 1 → Plg 2 → Plg 3. Presumably, coarser grains with high An content formed early and small grains with low An content formed late.

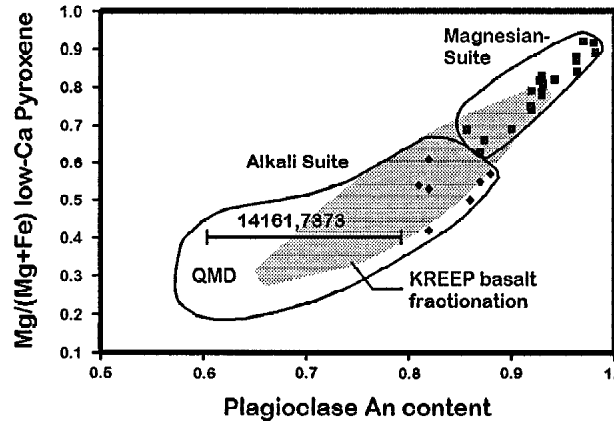

FIGURE 12. An content of plagioclase vs. cation proportions of Mg/(Mg+Fe) of low-Ca pyroxene in 14161,7373 compared to alkali and magnesian highland suites. Symbols represent analyses of many different rocks from the Apollo collections, taken from the literature. Superimposed on these fields is the approximate range of compositions corresponding to zoned grains of coexisting plagioclase and pyroxene in KREEP basalts and KREEP-like impact-melt rocks (unpublished data, Washington University) for which core compositions plot in the upper right and rims, lower left.

in the crystallizing assemblage. Assuming that the silicates co-crystallized with whitlockite, what do their REE concentrations indicate for the equilibrium-melt composition?

Before making this calculation, we question whether it is appropriate simply to divide by partition coefficients in the case of 14161,7373. This sample is not a cumulate that has been isolated from interaction with residual melt. One might argue that much of the assemblage is in fact residual melt. In this sample, the silicates may have at least partially equilibrated at near-solidus or subsolidus temperatures with a large proportion of whitlockite. Even so, we can compare the ratios of REE concentrations in different minerals to the ratios of the corresponding magmatic partition coefficients to assess the degree of equilibrium between different minerals.

Pyroxene REE concentrations vary significantly from grain to grain and between augite and pigeonite. The variations are complex and indicate that the pyroxenes are not well equilibrated with one another for the REE as they are for major elements. Factors that may complicate the distribution of REE in the pyroxene grains include variations in Wo content, the temperature range over which they first crystallized and subsequently exsolved, and the local assemblage with which they may have exchanged REE.

First we compare the REE concentrations in augite and pigeonite within a single exsolved grain: Pig 1 (Wo_8) is of host pigeonite and Aug 1 (Wo_{40}) is from a thick lamella adjacent to Pig 1 (Table 1). Mineral/melt partition coefficients for the REE have been calculated as a function of Wo content (e.g., McKay et al. 1986; Jones 1995) and are listed in Table 4, calculated for Wo contents corresponding to specific REE spot analyses. The measured augite/pigeonite concentration ratios range from ~6 for La to 1.7 for Lu and differ significantly from augite/pigeonite D-value ratios, which range from ~45 for La to ~3 for Lu (Fig. 13a). Partition coefficients for pigeonite and augite are temperature dependent such that at lower temperatures, partition coefficients are higher; however, augite/pigeonite REE ratios decrease (McKay and Weill 1976; Nielsen 1990). The decrease in augite/pigeonite ratios for the magmatic partition coefficients compared to Aug 1 and Pig 1 is roughly consistent with the difference between 1100 and 900 °C for the HREE, i.e., the range from magmatic crystallization to the estimated pyroxene-exsolution closure temperature in this rock. The difference for the LREE, however, is far greater, perhaps by as much as 4× the difference attributable simply to a decrease in temperature. Other natural augite-pigeonite pairs have been reported that have augite/pigeonite La ratios as high as 45 (e.g., Moore County: Pun and Papike 1995), thus there is no reason to suspect the experimental D-values. The departure from the experimental values of REE partitioning in this host-lamella pair is not resolved here, but we suggest that it is related in part to the temperature and rate of sub-solidus equilibration.

The same general relationship is evident in comparing the REE ratios between separate grains of augite and pigeonite whose compositions have been re-integrated (composite host

TABLE 4. Mineral/melt partition coefficients used in this study

	*Pig 1 $Wo_{7.6}$	Px1(c) $Wo_{13.3}$	Aug 1 $Wo_{39.8}$	Aug 2 $Wo_{33.3}$	Aug 3 $Wo_{41.0}$	Plagioclase
La	0.0010	0.0025	0.0478	0.0256	0.0537	0.0358
Ce	0.0023	0.0053	0.0720	0.0431	0.0791	0.0307
Pr	0.0045	0.0110	0.1082	0.0717	0.1168	0.0280
Nd	0.0077	0.0200	0.1477	0.1081	0.1564	0.0250
Sm	0.0160	0.0381	0.2304	0.1765	0.2420	0.0204
Eu	0.01	0.01	0.214	0.172	0.222	1.15
Gd	0.0232	0.0535	0.2502	0.1955	0.2619	0.0160
Tb	0.0322	0.0698	0.2608	0.2058	0.2724	0.0145
Dy	0.0433	0.0897	0.2699	0.2207	0.2801	0.0130
Ho	0.0572	0.1095	0.2793	0.2367	0.2880	0.0115
Y	0.0632	0.1184	0.2842	0.2451	0.2921	0.0107
Er	0.0698	0.1279	0.2891	0.2538	0.2962	0.0100
Tm	0.0829	0.1429	0.2993	0.2722	0.3045	0.0085
Yb	0.0953	0.1517	0.3097	0.2919	0.3132	0.0070
Lu	0.0997	0.1582	0.3184	0.2996	0.3220	0.0055

Notes: Partition coefficients for pigeonite and plagioclase calculated using the parameters of McKay et al. (1986). Plagioclase partition coefficients from Phinney and Morrison (1990); Eu in plagioclase and pigeonite from Jones (1995). Partition coefficients for REE not given in these references were interpolated.
*Column titles for pyroxene correspond to designations in text.

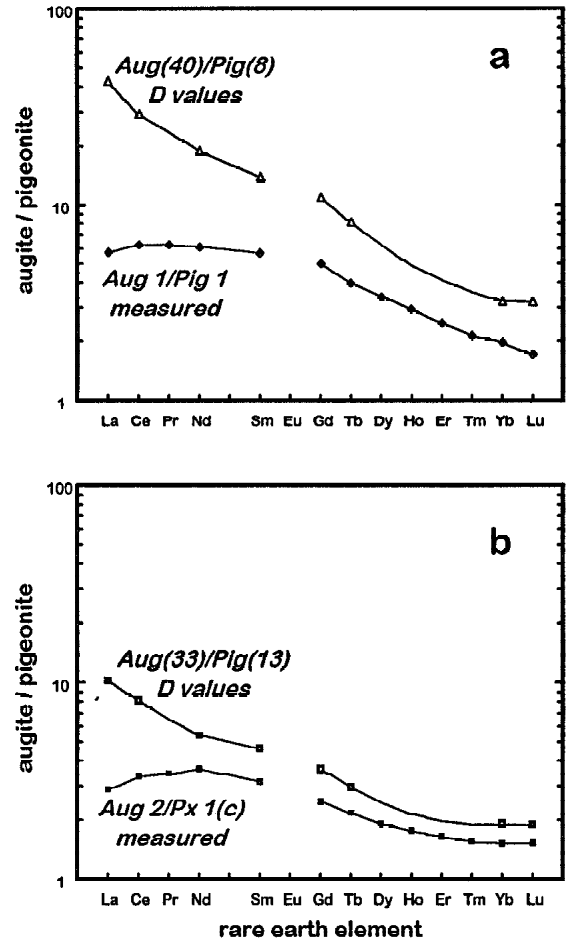

FIGURE 13. Augite/pigeonite REE ratios: comparison between natural pairs (measured) and augite/pigeonite REE D values, calculated for corresponding Wo contents (parameters from McKay et al. 1986). (a) The measured pair Aug 1/Pig 1 represent adjacent spot analyses of an augite lamella and pigeonite host (Table 1). (b) The pair Aug 2/Px 1(c) corresponds to a composite analysis of augite and a combined or "re-integrated" bulk pyroxene composition calculated as 80% Pig 1 plus 20% Aug 1. The Aug 2 analysis is mainly of the host augite in an exsolved grain, but includes ~20% overlap onto narrow pigeonite lamellae, making it a good approximation of the bulk augite. For the D-value ratios, the numbers in parentheses are the Wo content, and Pr and the HREE, Dy through Tm, are interpolated/estimated.

+ lamellae) as we found in comparing Aug 1/Pig 1 (exsolution lamella and host) to the experimental D_{REE} ratios. In this case, however, the differences are not as great (Fig. 13b). Here, we compare Aug 2 and Px 1(c), both of which are composite (re-integrated) compositions. Px 1(c) (Wo_{13}) was calculated by combining Pig 1 and Aug 1 in their observed proportions (measured by image analysis), and the Aug 2 (Wo_{33}) spot analysis overlapped augite host and pigeonite lamellae in approximately the same proportions as they occur in the augite grain. Overall, the augite/pigeonite REE ratios are lower for augite(Wo_{33})/pigeonite(Wo_{13}) than for augite(Wo_{40})/pigeonite(Wo_{8}) because the REE are increasingly compatible in pyroxene with increasing Wo content (McKay et al. 1986, see Fig. 13). The difference between the ratio for the composite grains and the corresponding experimental augite and pigeonite, however, is less than the difference between augite lamella/host pigeonite and their experimental counterparts (Fig. 13). This is consistent (in the right direction) with equilibration of the original augite and pigeonite grains at a higher temperature than for augite-pigeonite host-lamellae pairs (1100 vs. 850–900 °C, based on coexisting pyroxene compositions, Fig. 3). However, the ratios are still less than the experimental D-values, so temperature variations alone cannot fully explain the differences.

The downturn for augite/pigeonite LREE values in 14161,7373 pyroxene compared to the partition coefficients appears to be significant, but the reason for this is unclear at present. The distribution coefficients for the LREE in pigeonite are very low; the apparent discrepancy between 14161,7373 pyroxenes and experimental partition coefficients might mean that the partition coefficients are inappropriate for the specific conditions of this natural sample. Another possibility is that pigeonite was the earlier phase and incorporated higher REE concentrations (as would be the case if subsequent crystallization of whitlockite brought about a decrease in the REE concentration of residual melt). Then, during subsolidus cooling, the LREE were more sluggish to equilibrate than the HREE. A test of this possibility would require an evaluation of REE concentration profiles within individual grains and even within individual lamellae; however, such a test is beyond the scope of this work.

Given that Px 1(c), Aug 2, and Aug 3 spot analyses approximate bulk compositions of pyroxene grains, we compare the REE patterns of their calculated equilibrium melts in Figure 14a. Using D-values from Table 4, melt that would have been in equilibrium with Px 1(c) has the highest REE concentrations, and Aug 3 the lowest. Calculated equilibrium melts for Px 1(c) and Aug 2 are at or above KREEP concentrations and have flatter HREE slopes than KREEP (Fig. 14b). Px 1(c) also has a steeper LREE slope than KREEP (Fig. 14b). Aug 3, a small, interstitial grain lacking exsolution lamellae and intergrown with a eutectic assemblage of plagioclase, silica, and potassium feldspar, yields a

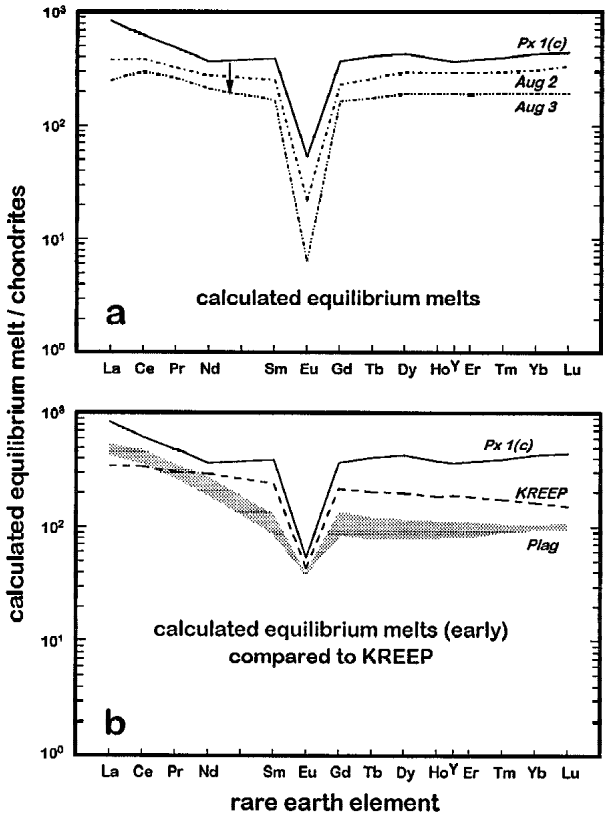

FIGURE 14. REE concentration of hypothetical melt in equilibrium with recombined coarse pigeonite grain, Px 1(c) (80% Pig 1 & 20% Aug 1), compared in **(a)** to augite (Aug 2 and Aug 3); and in **(b)** to plagioclase (range for Plg 1 and Plg 2), and high-K KREEP. The analysis of Aug 2 incorporated pigeonite in approximately the correct proportion (~20%) to represent a bulk analysis of that grain. Liquidus D values shown in Table 4 (McKay et al. 1986) were used to calculate equilibrium melt REE concentrations. If the sequence Px 1(c) → Aug 2 → Aug 3 corresponds to a decrease in temperature, the effect on calculated melt composition would be to further lower the REE concentrations of calculated melts because at lower temperatures, D_{REE} values for pyroxene increase (McKay and Weill 1976; Nielsen 1990).

lower calculated equilibrium-melt REE pattern; however, this calculation is relevant for the temperature of the liquidus partition coefficients. If Aug 3 formed or equilibrated at lower temperature, say 100–150 °C lower, near the solidus, as indicated by the local assemblage and its high Wo content (Wo_{41}), higher partition coefficients would be appropriate and the calculated equilibrium melt would have even lower REE concentrations than shown in Figure 14a. This is similar to the case for plagioclase where the most sodic, presumably latest-forming grain has the lowest REE concentrations (see below).

Plagioclase REE analyses record a range of compositions, indicating that plagioclase is not equilibrated (Fig. 11b). The three relatively calcic spot analyses, Plg 1, Plg 2a, and Plg 2b (An_{78}–An_{82}), yielded similar REE patterns. Plg 3, which is significantly more sodic (An_{62}) has the lowest REE concentrations. Two spot analyses on Plg 2, which is compositionally zoned, gave similar REE patterns, with slightly higher LREE concentrations on the less calcic (An_{78}) end of the grain. Using the Na_2O concentration as an indicator of crystallization sequence, we infer that the more calcic plagioclase crystallized early and the more sodic plagioclase, late. This is consistent with grain size; Plg 1 is the largest of the three and Plg 3, the smallest.

The REE concentrations in plagioclase are affected less by subsolidus structural modifications than they are for pyroxene, and therefore plagioclase may record variations in coexisting melt as the melt crystallized. Using partition coefficients from Phinney and Morrison (1990), we calculated the range of concentrations of REE in melt that would have been in equilibrium with the three relatively calcic plagioclase spot analyses (Fig. 14b), ignoring for the moment the differences among these three analyses. Compared to the melt that would have been in equilibrium with Px 1(c) composite pigeonite, the REE pattern of melt in equilibrium with plagioclase is substantially lower (~2× for La–Nd and 4× for Sm–HREE). Whether these differences are significant or simply reflect uncertainties in the partition coefficients appropriate to this assemblage is unclear. However, these differences hold open the possibility that early-formed, coarsely-exsolved, pyroxene is decoupled from (not in equilibrium with) the rest of the assemblage. Support for this comes from the texture of the coarse pyroxene grains, which appear to have been broken and rearranged, whereas the interstitial phases and the late-stage granophyric intergrowths appear to have formed in place. The discrepancy between calculated equilibrium melts for pyroxene and plagioclase may in part also relate to different crystallization temperatures. Partition coefficients for the REE in the two minerals are temperature dependent (McKay and Weill 1976; Nielsen 1990; Jones

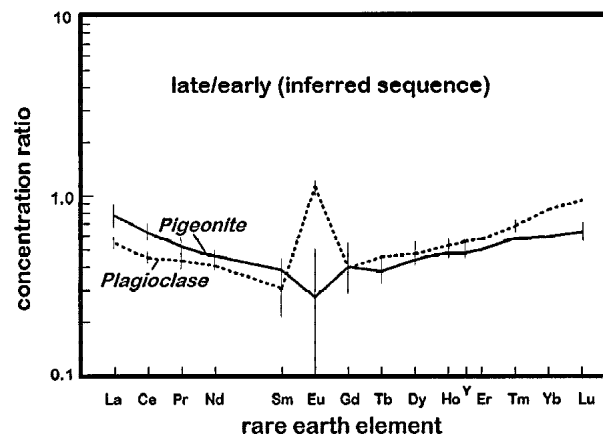

FIGURE 15. Late/early pyroxene and plagioclase REE patterns, showing the development of the V-shaped pattern in later-crystallizing grains due to the co-crystallization of whitlockite, which strongly partitions the middle REE. For this plot, REE concentrations in Pig 3 (late) are divided by those of Pig 1 (early). For plagioclase, REE concentrations are those of Plg 3 divided by Plg 2b. Error bars indicate the uncertainties in the ratios for Eu, based only on counting statistics. Ratios calculated for the trivalent REE use smoothed values (Figs. 7–10); one-sigma error bars shown for those ratios that did not involve a smoothed value.

1995), but in an opposite sense such that D_{REE}(plagioclase/melt) decrease and (pyroxene/melt) increase at lower T compared to conditions under which the most relevant published partition coefficients were obtained. Although the sense of change of D_{REE} with falling T is opposite for plagioclase and pyroxene, it is unlikely that this temperature effect would account for the magnitude of variations in REE concentrations early to late and it would not be expected to produce the same magnitude of variation among a group of pyroxene grains and a group of plagioclase grains. The decrease in REE concentrations of residual melt with crystallization that we infer from both plagioclase and pyroxene is more likely due to co-crystallization of whitlockite, which in this case draws down the REE.

Crystallization sequence and development of V-shaped REE patterns

On the basis of pyroxene and plagioclase grain sizes and on the Na_2O concentrations of plagioclase grains, we can infer the crystallization sequence. As discussed above, plagioclase grain size correlates with Na_2O concentration such that fine-grained interstitial plagioclase is the most sodic. These two features imply that the smaller, more sodic grains (e.g., Plg 3) formed late in the sequence. However, for pigeonite, there is nothing obvious about textures or major-element compositions to indicate the crystallization sequence, with the possible exception of decreasing Cr_2O_3 concentrations (0.21, 0.17, and 0.08 wt% in Pig 1, Pig 2, and Pig 3, respectively). By analogy with plagioclase, we assume that the highest REE concentrations occur in early pigeonite and the lowest, in late pigeonite. This is a reasonable assumption, because, as we discuss below, the onset of whitlockite crystallization prevented further enrichment of REE and probably caused REE concentrations to decrease in this assemblage as crystallization progressed.

Given this presumed early-to-late variation in REE concentrations, we show in Figure 15, using compositional ratios, an enhancement of the variation in REE patterns that accompanies the early-to-late crystallization sequence of the silicate assemblage. This figure demonstrates the middle-REE depletion and the development of a V-shaped pattern by comparing REE patterns of late/early plagioclase and presumed late/early pigeonite. In both pigeonite and plagioclase, the grains we infer to have formed late in the crystallization sequence have higher La/Sm and lower Gd/Lu than those formed early. The ratio of Eu in plagioclase (early/late) is about 1, suggesting no change in its concentration. In pigeonite, the low concentration of Eu probably renders the ratio meaningless for that element. The apparent extreme depletion of the REE in potassium feldspar (Fig. 11) makes a clear assessment impossible, but there is some indication that the potassium feldspar grains have been affected by the same apparent MREE depletion. By analogy to pigeonite and plagioclase, we might infer that the separate grain (Kfs 2), which is less depleted in MREE, formed before the one in the granophyric intergrowth (Kfs 1), but their differences might also reflect partitioning related to immiscible melt formation.

The atypically high proportion of whitlockite in this assemblage probably accounts for the MREE depletion observed in the silicates. With a high proportion of whitlockite, bulk REE

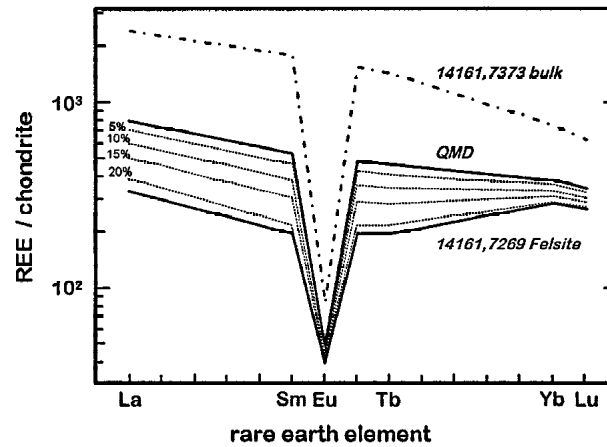

FIGURE 16. Calculated development of a V-shaped REE pattern in residual melt by subtraction of a whitlockite-rich mineral assemblage (after Fig. 11, Jolliff 1991). In this case, the "starting" melt has the REE pattern of a quartz-monzodiorite (QMD). Subtraction of increasing amounts of the whitlockite-rich assemblage, in this case, the bulk REE concentration of 14161,7373 determined by INAA, results in a shallow V-shape, which at 20% subtraction (by mass), closely matches the REE pattern of an actual felsite sample

distribution coefficients (mineral assemblage/melt) for the crystallizing assemblage likely exceeded 1 and REE concentrations would have decreased with the progressive crystallization of residual melt. Jolliff et al. (1993) calculated bulk distribution coefficients for this assemblage, by taking the constituent minerals in approximately eutectic proportions, to range from 0.52 (La) to 0.64 (Sm) to 0.37 (Lu); however, if the crystallizing assemblage had more whitlockite than the 5% used by Jolliff et al., or if the $D^{REE}_{whitlockite}$ values were higher than those calculated by Jolliff et al., then bulk distribution coefficients for the trivalent REE could have exceeded 1 and would have been highest in the MREE, excluding Eu.

Others have also concluded that the V-shaped REE pattern of most lunar granites resulted from fractionation of phosphates and not directly as a consequence of liquid-liquid partitioning accompanying SLI coupled with physical separation of the two liquids (e.g., Warren et al. 1983; Hess 1989; and Neal and Taylor 1989a–b). This is an important distinction: if either SLI or simply the crystallization of phosphates imposed a unique geochemical signature, then it might be possible to relate some of the largest granitic samples such as 12013 (Quick et al. 1981) and 14321,1027 (Warren et al. 1983), which do not have the corresponding conjugate mafic material, to an origin by one or the other processes. Longhi (1990, 1998) has argued that large volumes of high-silica melt are not likely to form by SLI and then separate and collect elsewhere because of their high viscosity (see also Hess et al. 1975; Neal and Taylor 1989c). Instead, when the mafic residual melt is mostly solidified, the remaining high-silica residual melt would show the geochemical effects of fractional crystallization. The scenario Longhi described is recorded in the textures and geochemistry of sample 14161,7373.

Figure 16 illustrates how a V-shaped REE pattern can be produced by crystallization of an assemblage with a high proportion of whitlockite (e.g., 8–10%). Starting with a melt of QMD-like

(or KREEP-like) REE proportions and concentrations, and subtracting an assemblage rich in whitlockite (the upper pattern in Figure 16, which is the bulk composition of sample 14161,7373), a V-shaped REE distribution results. At about 20% subtraction, the resulting melt REE pattern matches closely that of an actual lunar felsite bulk sample, including the V-shape and appropriate concentration levels. This results simply from the fractional crystallization of whitlockite; it appears to have nothing to do with SLI. However, if immiscibility follows, the granitic or high-silica fraction should show these effects; this may in fact be reflected by the two potassium feldspar REE patterns in 14161,7373.

In any case, the differences between early and late crystallizing silicates reflect co-crystallization of whitlockite, which caused a bowing downward of REE patterns and general depletion of REEs, especially the MREE, in late plagioclase and pigeonite. The Ba-rich potassium feldspar grains appear to record an extreme depletion of the MREE, consistent with their formation from late-stage residual melt (generic), in some cases, as part of granophyric segregations of felsic material whose textures indicate that the felsic material separated from mafic residual melt by SLI prior to their solidification (see below). In this assemblage, whitlockite crystallization preceded SLI.

Silicate liquid immiscibility

Jolliff (1991) argued that the compositions of the bulk sample, 14161,7373, and its granophyric intergrowths, are consistent with the granophyre having formed by separation of felsic, immiscible melt upon intersection of the bulk composition with the miscibility "dome" as the temperature decreased during crystallization (probably in the range of 975–1050 °C; see Hess et al. 1975; Hess 1989; Longhi 1990). This drove the composition of the conjugate residual melt fraction to become more mafic as it tracked down the limb of the solvus, resulting in a pyroxene and phosphate-rich assemblage. The bulk composition of 14161,7373, as measured by INAA, is not as strongly enriched, relative to KREEP, in those incompatible elements that tend to concentrate in lunar granite (e.g., Ba, Th, U, Ta, HREE) as it is in those that concentrate in whitlockite (LREE-MREE). Thus, despite the fact that felsic segregations (granophyre) occur in the assemblage, some fraction of felsic material appears to be missing. This is also evident by the disparity between the bulk major-element composition of sample 14161,7373 and the pseudoeutectic composition, which is more closely attained by other lunar QMD samples (e.g., Jolliff 1991; Snyder et al. 1995).

Because sample 14161,7373 is so small, we cannot say with certainty whether this assemblage represents a large-scale separation of the felsic fraction or whether it is just a non-representative sample of a larger rock where all the incompatible elements are present in QMD-like (or KREEP-like) proportions. The apparent shallow origin for this rock, however, seems more consistent with a small-scale separation. Perhaps immiscible felsic melt began to separate from the mafic melt as it crystallized slowly, but was partially lost when the assemblage was brought near to the surface, prior to final solidification. At least one sample, 14161,7269 (Jolliff 1991), occurs in the Apollo-14 regolith that contains quenched felsic (not impact) melt that is compositionally analogous to what we would expect for a granitic fraction lost from 14161,7373.

The unusual texture of silica containing an emulsion of sulfide blebs records another intriguing late-stage separation. Silica within granophyric intergrowths is free of troilite inclusions, whereas separate silica-rich masses contain as much as 5% of components other than SiO_2, mainly troilite (Fig. 2d). The occurrence of troilite blebs in silica appears to represent a very late stage separation of immiscible Fe-S-rich liquid from the highly siliceous fraction of residual melt. Based on this occurrence, we infer that similar occurrences of Fe-metal in silica, accompanied by vesicles, in the mesostasis of some KREEP basalts may have formed by degassing of a S-bearing species, e.g., H_2S or COS (Colson 1992), from erupted basalts. Whether this occurrence of troilite in silica is related to troilite plus silica filling fractures in pyroxene and whitlockite is uncertain, but possible.

PETROGENESIS-BASED ON COOLING RATES AND REE DISTRIBUTION

Pyroxene exsolution compositions and textures in 14161,7373 reflect a complex crystallization and recrystallization history. In the following suggested sequence of events, we place the complex compositional evolution of this assemblage, based on REE distribution among the minerals, within the context of settings suggested by pyroxene exsolution.

(1) At ~1100 °C (or somewhat higher) in a magma body in the lunar upper crust, growth and slow exsolution of pyroxene phenocrysts (pigeonite and minor augite) occurred, accompanied by plagioclase and possibly whitlockite, forming a microcumulus texture. The melt from which this rock crystallized may have been an alkali-suite melt, or a derivative of a magnesian-suite parent melt. The estimated REE concentrations of melt in equilibrium with early (bulk) pigeonite and augite range from ~1–2× high-K KREEP, similar to equilibrium melts calculated by Papike et al. (1996) for magnesian-suite norites. With continued slow cooling, relatively coarse exsolution textures developed in pyroxene. During this stage, it is possible that some pyroxene accumulation occurred (relative to plagioclase) because the two minerals are not in cotectic proportions. Whitlockite, based on its exceptionally high modal proportion, also may have accumulated during this stage. Crystallization of the whitlockite-rich assemblage led to a depletion of the MREE in residual melt that was recorded in the REE patterns of the silicates. The onset of SLI probably began near the end of this stage of slow cooling. For comparison, Rutherford et al. (1996) observed SLI in low-pressure experiments using a KREEP basalt composition at ~1040 °C and the onset of phosphate crystallization at 1026 °C (see also Longhi 1990).

(2) Prior to pigeonite inversion (~950–980 °C), and (incidentally) very near the final solidification temperature of felsic granophyre (~990 °C, see below), the rock from which 14161,7373 derived was transported closer to the lunar surface. Whether this event was caused by impact is uncertain; however, if it was, it took place in a part of the impact regime that was not so energetic as to disrupt the assemblage completely and mix it with other rocks. Perhaps this event occurred in an area that was not excavated, but was part of a rebound-uplift structure. This event resulted in fracturing and mechanical and/or chemical erosion of pyroxene, as well as early-formed coarse plagioclase and whitlockite. The smooth, unbroken ovoid shapes of granophyric intergrowths suggest that they solidified

after this event. Judging from the bulk major- and trace-element composition of 14161,7373, a portion of the immiscible felsic melt was lost from the assemblage. If residual melt—either the felsic immiscible fraction or post-immiscibility, silicic residual melt—was still liquid during this relocation event, then perhaps some of this melt was separated by a process of filter pressing.

(3) Relocation to near the surface was accompanied by reheating (recorded by perturbations in the pyroxene exsolution), most likely due to impact. This thermal pulse may have caused remelting of interstitial material, and the formation of troilite veins.

(4) A period of fairly rapid cooling and crystallization (most likely in an ejecta blanket) followed to produce the textures we now see. Troilite blebs in late-stage silica record the exsolution of FeS from a very-late residual melt, arrested in progress.

(5) The last major event to affect this sample was excavation by an impact cratering event, which caused re-fracturing of all minerals, and delivery of the sample to the Apollo 14 regolith.

The preservation of the ovoid granophyric segregations seems to require special circumstances. The fact that pigeonite did not invert to orthopyroxene indicates that temperatures during the slow cooling phase did not get much below the pigeonite decomposition temperature. For pigeonite with the composition $En_{34.4}$ $Fs_{51.2}$, the minimum stability at low pressure is probably in the range 950–980 °C (Brown 1972; Ishii 1975), but possibly as low as 900 °C (Huebner 1980; Sack and Ghiorso 1994). Pigeonite could survive metastably below the inversion temperature, but it is unlikely that the temperature got below 850–900 °C. This is significant because the potassium feldspar + silica assemblage, e.g., in the ovoid granophyres, would be crystalline at temperatures less than about 990 °C, based on the data of Schairer and Bowen (1955) for the anhydrous system potassium feldspar + tridymite. Thus, unless some component or combination of components such as Cl, F, or S lowered the eutectic temperature, it is likely that the granophyric material would have been crystalline by the end of the period of slow cooling. If this were so, then how would the granophyres retain their pristine shape through an impact disruption? Perhaps if reheating during stage 3 raised the temperature to near 1000 °C, then most of the intercumulus material along with unmixed silica-rich material might have been remelted. Subsequent recrystallization of the granophyres and the crystallization of the late stage interstitial material molded around the ovoids (mainly whitlockite-apatite-ilmenite-plagioclase-troilite) would then have occurred after the final emplacement. The intergrowth textures of potassium feldspar and silica in the granophyres are common in shallow-level terrestrial intrusions such as the Skaergaard, where granophyre also occurred as a result of late-stage immiscible-melt separation (McBirney 1996). Perhaps the granophyres were fully solidified during the stage of slow cooling and simply survived brecciation. Even so, reheating during stage 3 may have melted/recrystallized the latest-stage interstitial assemblage.

Whether or not our interpretation of the precise history of this sample is correct, it is clear that its origin was shallow—in the upper crust of the Moon, near the surface. Near-surface origins are also indicated by cooling-rate studies of QMD in 15403 (O'Brien and McCallum 1996). The common association of QMD and granite in lunar samples is reminiscent of the association of granophyre and fractionated basalt in terrestrial, near-surface intrusive bodies, and this association indicates shallow origins for the granites as well. Sample 14161,7373, although small, provides compelling evidence that silicate-liquid immiscibility occurred to form granophyric segregations in a shallow intrusive setting, at a depth of less than a kilometer. Although the results of experimental studies indicate that SLI at greater depths, perhaps even at the base of the crust, is expected (Hess et al. 1975; Longhi 1990) and possible (Rutherford et al. 1996), we do not yet know if separation of felsic material by immiscibility from KREEP-like residual melts and accumulation of that material also occurred deep in the crust of the Moon. In the melt parental to sample 14161,7373, SLI occurred late in the crystallization sequence, after the onset of whitlockite crystallization. The crystallization of whitlockite caused a depletion of the MREE in late crystallizing phases and residual melt; this fractionation can produce the V-shaped REE pattern that is typical of lunar granitic materials. There is evidence in 14161,7373 that partial physical separation of the felsic fraction from the mafic assemblage occurred on a scale at least larger than this sample, but we still do not know the possible extent of such separations in ancient lunar magmatic environments.

ACKNOWLEDGMENTS

We thank Alian Wang (Wash U.) for Raman-spectroscopic measurements and Scott Kuehner (U. Wash) for assistance with the microprobe analyses. Hugh O'Brien provided invaluable assistance in development of the cooling-rate models. Detailed reviews by Paul Warren and Greg Snyder helped considerably to improve the manuscript and their efforts are appreciated. Funding for this work was provided by NASA grants NAGW-3343 to L.A. Haskin (B.L.J.), NAGW-3371 to G. Crozaz (C.F.), and NAGW-3352 to I.S. McCallum (I.S.M. and J.M.S.).

REFERENCES CITED

Anders, E. and Grevesse, N. (1989) Abundances of the elements: Meteoritic and solar. Geochimica et Cosmochimica Acta, 53, 197–214.

Brown, G.M. (1972) Pigeonitic pyroxenes: A review. Geological Society of America Memoir, 132, 523–534.

Colson, R.O. (1992) Mineralization on the Moon? Theoretical considerations of Apollo 16 "rusty rocks," sulfide replacement in 67016, and surface-correlated volatiles on lunar volcanic glass. Proceedings of Lunar and Planetary Science, 22, 427–436.

Drake, M.J. and Weill, D.F. (1972) New rare earth standards for electron microprobe analysis. Chemical Geology, 10, 179–181.

Floss, C. and Jolliff, B.L. (1998) Rare earth element sensitivity factors in calcic plagioclase (anorthite). Proceedings of the Eleventh International Conference on Secondary Ion Mass Spectrometry (SIMS XI), Orlando, Florida, Sept. 1997.

Floss, C., Strait, M.M., and Crozaz, G. (1990) Rare earth elements and the petrogenesis of aubrites. Geochimica et Cosmochimica Acta, 54, 3553–3558.

Floss, C., James, O.B., McGee, J.J., and Crozaz, G. (1997) Lunar ferroan anorthosite petrogenesis: Clues from trace element distributions in FAN subgroups. Geochimica et Cosmochimica Acta, 62, 1255–1283.

Ganguly, J. and Tazzoli, V. (1994) Fe^{2+}-Mg interdiffusion in orthopyroxene: Retrieval from the data on intracrystalline exchange reaction. American Mineralogist, 79, 930–937.

Ganguly, J., Bhattacharya, R.N., and Chakraborty, S. (1988) Convolution effects in the determination of compositional profiles and diffusion coefficients by microprobe step scans. American Mineralogist, 73, 901–909.

Hess, P.C. (1989) Highly evolved liquids from the fractionation of mare and nonmare basalts. In Workshop on Moon in Transition: Apollo 14 KREEP, and Evolved Lunar Rocks (G.J. Taylor and P.H. Warren, eds.), 46–52. LPI Technical Report 89-03. Lunar and Planetary Institute, Houston.

Hess, P.C., Rutherford, M.J., Guillemette, R.N., Ryerson, F.J., and Tuchfeld, H.A. (1975) Residual products of fractional crystallization of lunar magmas: An experimental study. Proceedings of the Sixth Lunar Science Conference, Geochimica et Cosmochimica Acta Supplement 6, 895–909

Hess, P.C., Horzempa, P., and Rutherford, M.J. (1989) Fractionation of Apollo 15

KREEP basalts. In Lunar and Planetary Science XX, p. 408–409. Lunar and Planetary Institute, Houston, Texas.
Horai, K. and Winkler, J.L. (1976) Thermal diffusivity of four Apollo 17 rock samples. Proceedings of the Seventh Lunar Science Conference, Geochimica et Cosmochimica Acta Supplement 7, 3183–3204.
Huebner, J.S. (1980) Pyroxene phase equilibria at low pressure. In Mineralogical Society of America Reviews in Mineralogy, 7, 213–288.
Irvine, T.N. (1970) Heat transfer during solidification of layered intrusions. I. Sheets and sills. Canadian Journal of Earth Science, 7, 1031–1061.
Ishii, T. (1975) The relations between temperature and composition of pigeonite in some lavas and their application to thermometry. Mineralogical Journal, 8, 48–57.
Jaeger, J.C. (1968) Cooling and solidification of igneous rocks. In H.H. Hess and A. Poldervaart, Eds., Basalts 2, p. 503–536. Interscience Publishers, New York.
Jolliff, B.L. (1991) Fragments of quartz monzodiorite and felsite in Apollo 14 soil particles. Proceedings of Lunar and Planetary Science, 21, 101–118.
——— (1998) Large-scale separation of K-frac and REEP-frac in the source regions of Apollo impact-melt breccias and a revised estimate of the KREEP composition. International Geology Review, 40, 916–935.
Jolliff, B.L. and Hsu, W. (1996) Geochemical effects of recrystallization and exsolution of plagioclase of ferroan anorthosites. In Lunar and Planetary Science XXVII, p. 611–612. Lunar and Planetary Institute, Houston, Texas.
Jolliff, B.L., Korotev, R.L., and Haskin, L.A. (1991) Geochemistry of 2–4 mm particles from Apollo 14 soil (14161) and implications regarding igneous components and soil-forming processes. Proceedings of Lunar and Planetary Science, 21, 193–219.
Jolliff, B.L., Haskin, L.A., Colson, R.O., and Wadhwa, M. (1993) Partitioning in REE-saturating minerals: Theory, experiment, and modeling of whitlockite, apatite, and evolution of lunar residual magmas. Geochimica et Cosmochimica Acta, 57, 4069–4094.
Jones, J.H. (1995) Experimental trace-element partitioning. In Rock Physics and Phase Relations, A Handbook of Physical Constants. American Geophysical Union Reference Shelf 3.
Longhi, J. (1981) Preliminary modeling of high pressure partial melting: Implications for early lunar differentiation. Proceedings of the Twelfth Lunar and Planetary Science Conference, Part B, Supplement 16, 1001–1018.
——— (1989) Fractionation trends of evolved lunar magmas. In Lunar and Planetary Science XX, 584–585. Lunar and Planetary Institute, Houston, Texas.
——— (1990) Silicate liquid immiscibility in isothermal crystallization experiments. Proceedings of the Twentieth Lunar and Planetary Science Conference, Geochemica et Cosmochimica Acta, Supplement 16, 13–24.
——— (1991) Comparative liquidis equilibria of hypersthene-normative basalts as low pressure. American Mineralogist, 76, 785–800.
——— (1998) Silicate liquid immiscibility: A furtive agent of fractionation. In Lunar and Planetary Science XXIX, No. 1903, Lunar and Planetary Institute, Houston.
Marvin, U.B., Holmberg, B.B., and Lindstrom, M.M. (1990) New pieces of the lunar granite-quartz monzodiorite puzzle. In Lunar and Planetary Science XXI, 408–409. Lunar and Planetary Institute, Houston, Texas.
McBirney, A.R. (1996) The Skaergaard Intrusion. In R.G. Cawthorn, Ed., Layered Intrusions, p. 147–180. Elsevier, Amsterdam.
McCallum, I.S. and O'Brien, H.E. (1996) Stratigraphy of the lunar highland crust: Depth of burial of lunar samples from cooling rate studies. American Mineralogist, 81, 1166–1175
McKay, G.A., and Weill, D.F. (1976) Petrogenesis of KREEP. Proceedings of the Seventh Lunar Science Conference, Geochemica et Cosmochimica Acta Supplement 7, 2427–2447.
McKay, G., Wagstaff, J., and Yang, S.-R. (1986) Clinopyroxene REE distribution coefficients for shergottites: The REE content of the Shergotty melt. Geochimica et Cosmochimica Acta, 50, 927–937.
Morris, R.W., Taylor, G.J., Newsom, H.E., Keil, K., and Garcia, S.R. (1990) Highly evolved and ultramafic lithologies from Apollo 14 soils. Proceedings of the Twentieth Lunar and Planetary Science Conference, Houston, 61–75.
Neal, C.R. and Taylor, L.A. (1989a) The nature of barium partitioning between immiscible melts: A comparison of experimental and natural systems with reference to lunar granite petrogenesis. Proceedings of the Nineteenth Lunar and planetary Science Conference, 209–218.
——— (1989b) Lunar granite petrogenesis and the Process of Silicate Liquid Immiscibility: The barium problem. In G.J. Taylor and P.H. Warren, Eds., Workshop on Moon in Transition: Apollo 14, KREEP, and Evolved Lunar Rocks, p. 89–93. LPI Technical Report 89-03. Lunar and Planetary Institute, Houston, Texas.
——— (1989c) The splitting of KREEP into identifiable components: The "K-frac" and "REEP-frac" hypothesis. In G.J. Taylor and P.H. Warren, Eds., Workshop on Moon in Transition: Apollo 14, KREEP, and Evolved Lunar Rocks, p. 94–99. LPI Technical Report 89-03. Lunar and Planetary Institute, Houston, Texas.
——— (1991) Evidence for metasomatism of the lunar highlands and the origin of whitlockite. Geochimica et Cosmochimica Acta, 55, 2965–2980.
Nielsen, R. (1990) Modern Methods of Igneous Petrology. In Mineralogical Society of America Reviews In Mineralogy, 24, 65–106.
O'Brien, H.E. and McCallum, I.S. (1996) The depth of formation of highly evolved lunar rocks. In Lunar and Planetary Science XXVII, 975–976.
Papike, J.J., Fowler, G.W., and Shearer, C.K. (1994) Orthopyroxene as a recorder of lunar crust evolution: Am ion microprobe investigation of Mg-suite norites. American Mineralogist, 79, 796–800.
Papike, J.J., Fowler, G.W., Shearer, C.K., and Layne, G.D. (1996) Ion microprobe investigation of plagioclase from lunar Mg-suite norites: Implications for calculating parental melt REE concentrations and for assessing post-crystallization REE distribution. Geochimica et Cosmochimica Acta, 60, 3967–3978.
Phinney, W.C. and Morrison, D.A. (1990) Partition coefficients for calcic plagioclase: Implications for Archean anorthosites. Geochimica et Cosmochimica Acta, 54, 1639–1654.
Pun, A. and Papike, J.J. (1995) Ion microprobe investigation of exsolved pyroxenes: Determination of minor and trace-element partition coefficients. Geochimica et Cosmochimica Acta, 59, 2279–2289.
Quick, J.E. and Albee A.L. (1976) 12013 revisited–Two clast-laden melts. In Lunar Science VII, p. 712–714. The Lunar Science Institute, Houston.
Quick, J.E., Albee A.L., Ma, M.-S., Murali, A.V., and Schmitt, R.A. (1977) Chemical compositions and possible immiscibility of two silicate melts in 12013. Proceedings of the Eighth Lunar Science Conference, Geochemica et Cosmochimica Acta Supplement 8, 2153–2189.
Quick, J.E., James, O.B., and Albee, A.L. (1981) Petrology and petrogenesis of lunar breccia 12013. Proceedings of the Twelfth Lunar and Planetary Science Conference, Geochimica et Cosmochimica Acta Supplement 16, 117–172.
Roedder, E. and Weiblen, P.W. (1971) Petrology of silicate melt inclusions, Apollo 11 and 12 and terrestrial equivalents. Proceedings of the Second Lunar Science Conference, Geochimica et Cosmochimica Acta Supplement 2, 507–528.
Rutherford, M.J., Hess, P.C., Ryerson, F.J., Campbell, H.W., and Dick, P.A. (1976) The chemistry, origin, and implications of lunar granite and monzodiorite. Geochimica et Cosmochimica Acta Supplement 7, 1723–1740.
Rutherford, M.J., Tonks, B., and Holmberg, B. (1996) Experimental study of KREEP basalt evolution: The origin of QMD and granite at the base of the lunar crust. In Lunar and Planetary Science XXVII, 1113–1114.Lunar and Planetary Institute, Houston, Texas.
Ryder, G. (1976) Lunar sample 15405: Remnant of a KREEP basalt-granite differentiated pluton. Earth and Planetary Science Letters, 29, 255–268.
———(1992) Chemical variation and zoning of olivine in lunar dunite: Near-surface accumulation. Proceedings of Lunar and Planetary Science, 22, 373–380.
Sack, R.O. and Ghiorso, M.S. (1994) Thermodynamics of multicomponent pyroxenes: II. Phase relations in the quadrilateral. Contributions to Mineralogy and Petrology, 116, 287–300.
Schairer, J.F. and Bowen, N.L. (1955) The system K_2O-Al_2O_3-SiO_2. American Journal of Science, 253, 681–746.
Shervais, J.W., Taylor, L.A., Laul, J.C., Shih, C.-Y., and Nyquist, L.E. (1985) Very high potassium (VHK) basalt: Complications in mare basalt petrogenesis. Proceedings of the Sixteenth Lunar and Planetary Science Conference. Journal of Geophysical Research, 90, D3–D18.
Snyder, G.A., Taylor, L.A., and Halliday, A.N. (1995) Chronology and petrogenesis of the lunar highlands alkali suite: Cumulates from KREEP basalt crystallization. Geochimica et Cosmochimica Acta, 59, 1185–1203.
Spudis, P.D. (1993) The Geology of Multi-Ring Impact Basins, 263 p. Cambridge University Press, New York.
Taylor, G.J., Warner, R.D., Keil, K., Ma, M.-S., and Schmitt, R.A. (1980) Silicate liquid immiscibility, evolved lunar rocks and the formation of KREEP. In J.J. Papike and R.B. Merrill, Eds., Proceedings of the Conference on the Lunar Highlands Crust, p. 339–352. Pergamon, New York.
Warren, P.H. (1988) KREEP: Major-element diversity, trace-element uniformity (almost). In G.J. Taylor and P.H. Warren, Eds., Workshop on Moon in Transition: Apollo 14, KREEP, and Evolved Lunar Rocks, p. 106–110. LPI Technical Report 89-03. Lunar and Planetary Institute, Houston, Texas.
——— (1993) A concise compilation of petrologic information on possibly pristine nonmare Moon rocks. American Mineralogist, 78, 360–376.
Warren, P.H., Taylor, G.J., Keil, K., Shirley, D.N., and Wasson, J.T. (1983) Petrology and chemistry of two "large" granite clasts from the Moon. Earth and Planetary Science Letters, 64, 175–185.
Warren, P. H., Haack, H., and Rasmussen, K.L. (1991) Megaregolith insulation and the duration of cooling to isotopic closure within differentiated asteroids and the Moon. Journal of Geophysical Research, 96, 5909–5923.
Zinner, E. and Crozaz, G. (1986) A method for the quantitative measurement of rare earth elements in the ion microprobe. International Journal of Mass Spectrometry and Ion Processes, 69, 17–38.

MANUSCRIPT RECEIVED JANUARY 29, 1998
MANUSCRIPT ACCEPTED DECEMBER 17, 1998
PAPER HANDLED BY ADRIAN BREARLEY